2013

The Effects of Blockage Ratio and Distance from a Free Surface on the Performance of a Hydrokinetic Turbine

Peter Michael Creciun
Lehigh University

The Effects of Blockage Ratio and Distance from a Free Surface on the Performance of a Hydrokinetic Turbine

by

Peter Creciun

A Thesis

Presented to the Graduate and Research Committee

of Lehigh University

in Candidacy for the Degree of

Master of Science

in

Mechanical Engineering

Lehigh University

September 2013

This thesis is accepted and approved in partial fulfillment of the requirements for the Master of Science in Mechanical Engineering.

_____
Date Approved

_____
Dr. Alparslan Oztekin

_____
Dr. D. Gary Harlow, Chairperson
Mechanical Engineering and Mechanics

Table of Contents

List of Figures

Acknowledgements

The author wishes to express appreciation to his advisor, Professor Alparslan Oztekin, for his encouragement and assistance in researching the topic of this paper. He would also like to thank colleagues Chris Schleicher and Jake Riglin for their help in working with ANSYS and related software. Such help was truly invaluable and made possible the swift completion of this thesis.

Nomenclature

B	Blockage Ratio [-]
$D_{H,t}$	Turbine Hydraulic Diameter [m]
$D_{H,c}$	Channel Hydraulic Diameter [m]
A_t	Turbine Cross-sectional Area [m^2]
A_c	Channel Cross-sectional Area [m^2]
h	Turbine Depth [m]
t	Time [s]
ρ	Density [kg m^{-3}]
k	Turbulence Kinetic Energy [m^2 s^{-2}]
x	Position Vector [m]
u	Velocity Vector [m s^{-1}]
Γ_k	Effective Diffusivity of k [kg m^{-1} s^{-1}]
$\widetilde{G_k}$	Generation of k [kg m^{-1} s^{-3}]
Y_k	Dissipation of k [kg m^{-1} s^{-3}]
S_k	Source Term [kg m^{-1} s^{-3}]
ω	Specific Dissipation Rate [s^{-1}]
Γ_ω	Effective Diffusivity of ω [kg m^{-1} s^{-1}]
G_ω	Generation of ω [kg m^{-3} s^{-2}]
Y_ω	Dissipation of ω [kg m^{-3} s^{-2}]
D_ω	Cross-Diffusion Term [kg m^{-3} s^{-2}]
S_ω	Source Term [kg m^{-3} s^{-2}]
μ	Dynamic Viscosity [kg m^{-1} s^{-1}]
μ_t	Turbulent Dynamic Viscosity [kg m^{-1} s^{-1}]
σ_k	Turbulent Prandtl Number for k [-]
σ_ω	Turbulent Prandtl Number for ω [-]
F_1	Blending Function [-]
$\sigma_{k,1}$	Constant [1.176]
$\sigma_{k,2}$	Constant [2.0]
$\sigma_{\omega,1}$	Constant [1.0]
$\sigma_{\omega,2}$	Constant [1.168]
α^*	Correction Coefficient [-]
S	Magnitude of Mean Rate-of-Strain Tensor [-]
F_2	Blending Function [-]
a_1	Constant [0.31]
α^*_∞	Constant [1]
α^*_0	Parametric Constant [-]
Re_t	Turbulent Reynolds Number [-]
R_k	Constant [6]
β_i	Parametric Constant [-]
$\beta_{i,1}$	Constant [0.075]
$\beta_{i,2}$	Constant [0.0828]
S_{ij}	Mean Rate-of-Strain Tensor [-]
Φ_1	Parametric Constant [-]

y	Distance to Next Surface [m]
D_ω^+	Positive Portion of Cross-Diffusion Term [kg m^{-3} s^{-2}]
Φ_2	Parametric Constant [-]
G_k	Generation of k [kg m^{-1} s^{-3}]
β^*	Parametric Constant [-]
β_i^*	Parametric Constant [-]
ζ^*	Constant [1.5]
M_t	Turbulent Mach Number [-]
β_∞^*	Constant [0.09]
R_β	Constant [8]
M_{t0}	Constant [0.25]
a	Speed of Sound [m s^{-1}]
ν_t	Turbulent Kinematic Viscosity [m^2 s^{-1}]
α	Parametric Constant [-]
α_∞	Parametric Constant [-]
α_0	Constant [1/9]
R_ω	Constant [2.95]
$\alpha_{\infty,1}$	Parametric Constant [-]
$\alpha_{\infty,2}$	Parametric Constant [-]
κ	Constant [0.41]
∇	Vector Differential Operator [-]
$\bar{v}_r$	Relative Velocity Vector [m s^{-1}]
$\bar{\omega}$	Angular Velocity Vector [rad s^{-1}]
$\bar{r}$	Position Vector [m]
P	Pressure [Pa]
$\bar{\bar{\tau}}_r$	Viscous Stress Tensor [Pa]
$\bar{F}$	External Force Vector per Unit Length [N m^{-1}]
$\bar{u}$	Average Local Velocity [m s^{-1}]
U	Maximum Velocity [m s^{-1}]
r	Local Radius [m]
R	Channel Radius [m]
n	Parametric Constant [-]
Re_U	Reynolds Number based on Maximum Velocity [-]
I	Turbulence Intensity [-]
Re_{D_H}	Reynolds Number based on Hydraulic Diameter [-]
D_H	Hydraulic Diameter [m]
u_{avg}	Average Flow Velocity [m s^{-1}]
C_μ	Specified Empirical Constant [≈0.09]
l	Turbulence Length Scale [m]
C_p	Coefficient of Performance [-]
P_E	Power Extracted [W]
P_A	Power Available [W]
T	Torque [N m]
ω_f	Turbine Angular Velocity [rad s^{-1}]
z	z-coordinate [m]

Abstract

Blockage ratio and distance below a free surface are two factors that potentially affect hydrokinetic turbine performance. The extent of the effects of these parameters is considered by determining the coefficient of performance of a simple turbine blade rotating at 250 RPM in a 3.5-m/s flow of water using FLUENT Computational Fluid Dynamics software. The effects of blockage ratio are tested in a circular duct of varying diameter (0.5588 to 10.668 meters (22 to 420 inches)), while the effects of distance below a free surface are tested in a river bed, where the depth of the turbine is varied (0.3175 to 4.1148 meters (12.5 to 162 inches)). The coefficient of performance is shown to vary only slightly for values of blockage ratio below about 0.4. As the blockage ratio increases beyond 0.4, the coefficient of performance increases greatly and graphically tends toward a vertical asymptote as the blockage ratio approaches 1. Turbine depth is shown to have little or no effect on a turbine's coefficient of performance, except when the turbine is very close to the surface, at which point the coefficient of performance increases; however, the model or mesh employed to obtain these results may not be sufficient. It is suggested that a finer mesh or a two-phase model including air above the river be used in the further study of this topic.

1. Introduction

1.1 Hydropower

Hydropower has been a source of energy for at least 2000 years, having been used in ancient China, Greece, and Rome. More recently, around the year 1500, waterwheels were widely used in Europe to power a number of machines, including grain mills, mining elevators, and bellows in iron works [1]. With the construction of dams and power plants in the United States in the late 1800s and early 1900s, hydropower became a significant source of electricity to the growing nation. At one point during this time, over forty percent of the country's electricity came from hydroelectric power; however, today this number is down to around ten percent [2] [3].

Renewable energy is a topic of interest in today's world, and hydropower is such a source of energy, relying on the natural water cycle. Hydropower is also a source of "clean" energy, producing no carbon dioxide and causing no air pollution [4]. However, there are also certain environmental drawbacks to using some common forms of hydropower, such as dams and pumped storage facilities. Both of these types of facilities can affect the water flowing downstream, distorting its quality and quantity, thus affecting plant and animal life. Dams can block migration routes of marine animals, and the construction of new dams can destroy both plant and animal habitats [4].

One specific and more recent hydropower system is the hydrokinetic turbine. Unlike conventional hydropower systems that require a head (or vertical drop) of water

across the turbine, hydrokinetic turbines generate electricity from the flow of water in the channel in which they are placed [5]. This means that, for a small enough hydrokinetic system, any river, stream, or other decently-sized flowing body of water can act as a source of hydropower. Additionally, since a vertical drop across the turbine is not needed, dam-like structures do not have to be built, greatly reducing effects on the environment.

Hydrokinetic turbines are classified into two types: (1) horizontal axis turbines, whose rotational axis lies parallel to the flow direction, and (2) vertical axis turbines, whose rotational axis lies perpendicular to the flow direction [6] [7] [8] [9]. Vertical axis turbines tend to have lower efficiencies than horizontal axis turbines. This is because the blades on vertical axis turbines continually change angle as they rotate, providing less-than-optimal lift for part of each cycle, thus decreasing efficiency [10]. Therefore, this study focuses on the use of horizontal axis turbines.

1.2 Blockage Ratio and Free Surface

It is important to study how different factors affect hydrokinetic turbine performance. One such factor is blockage ratio, which is defined in this report as

$$B = \frac{D_{H,t}}{D_{H,c}}, \tag{1}$$

where B is the blockage ratio; $D_{H,t}$ is the hydraulic diameter of the turbine; and $D_{H,c}$ is the hydraulic diameter of the channel.

The maximum possible efficiency achievable by a turbine is commonly known as the Betz limit, having a value of 16/27 (or 0.593). Yet, Garrett and Cummins [11] determined in a 2007 analytical study that the maximum efficiency of a single turbine with a cross-sectional area A_t in a channel with a uniform cross-sectional area of A_c is $(16/27)(1 - A_t/A_c)^{-2}$. According to [11], the additional efficiency is due to the presence in their calculations of a confining channel. As $A_t/A_c \to 0$, i.e. an infinite medium, their maximum efficiency approaches the Betz limit.

Another factor that may influence hydrokinetic turbine performance is the depth of the turbine below the free surface of a channel, referred to in this paper as h and measured from the centerline of the turbine. In an application where the turbine is placed in a river or other natural body of water, the lack of a wall on the top surface of the channel could have its own effects on the power produced by the turbine. As such, the effects of the variation of this parameter are a topic of interest.

This thesis focuses on the effects that blockage ratio and distance from a free surface have on the performance of a single hydrokinetic turbine. Two models are considered in this study: (1) a turbine in a circular duct of varying diameter to examine the effect of blockage ratio and (2) a turbine in a constant-diameter river, where the position of the turbine varies to determine the effect of the presence of the free surface. The method used to determine these performance effects is computational fluid dynamics.

1.3 Computational Fluid Dynamics

Computational fluid dynamics (CFD) is a tool used to determine approximate solutions to heat transfer and fluid dynamics problems by way of numerical methods [12]. Its earliest uses involved the solving of one-dimensional equations for military problems in the first half of the twentieth century; these problems were solved by hand with the help of tables. With the aid of computers, two- and three-dimensional problems were being solved by the end of the 1960s and the 1980s, respectively [12]. Today, numerous students and professionals use CFD on a daily basis.

The use of CFD involves a series of steps. First, the model geometry must be created. This step is typically done with Computer-Aided Design (CAD) modeling software, such as SolidWorks, AutoCAD, or (as in this study) ANSYS DesignModeler. Once the geometry is created, a grid (or mesh) must be produced for it. The user must determine an appropriate number of elements to be used in the mesh. Having more elements generally leads to a more accurate solution, but adding more elements also increases computational time. The user should try to find a balance that provides accurate results in a reasonable amount of time.

Next, numerical models must be chosen to accurately simulate the problem. For example, in a pipe flow problem one would consider whether the problem is transient or steady-state and whether the flow is laminar or turbulent. Then, boundary conditions are applied to the problem. Parameters at the inlet and outlet can be specified, as well as conditions of the computational domain walls.

After these steps have been completed, the solution is ready to be calculated. Multiple codes exist for performing this step; these include FLUENT, STAR-CD, and OpenFOAM. Certain inputs can be specified in this step, such as the number of iterations to perform. However, reaching the number of iterations specified does not mean that the solution has converged. Values, such as maximum cell residuals and properties of interest (e.g. coefficient of drag and mass flow rate) should be monitored at each iteration. As the solution approaches the specified number of iterations, residuals should approach zero, and properties of interest should approach expected or at least reasonable values.

Finally, once the solution has been calculated, post-processing can take place. In this step, the results of the simulation can be viewed: velocity and pressure contours can be displayed; vector plots can be generated; performance values can be calculated; etc. One must make sure that the results displayed in this step are reasonable and make physical sense; otherwise, the solution may not be valid.

2. Geometry and Mesh

2.1 Computational Domain

Two computational domains are employed in this study, one for each part of the problem. The first domain is a circular duct, whose diameter varies from 0.5588 to 10.668 meters (22 to 420 inches) in order to alter the blockage ratio. The rotor of the turbine blade is aligned with the centerline of the duct, and the turbine is located within the duct such that the distance upstream of the blade is 0.762 meters (30 inches) and the distance downstream is 3.81 meters (150 inches). Figure 1 shows this domain with the turbine inside, where the duct diameter is 2.667 meters (105 inches).

The total computational domain for the second part of this problem consists of two subdomains: a turbine subdomain and a river subdomain. The turbine subdomain is a cylinder with a diameter of 1.6002 meters (63 inches) and a length of 3.81 meters (150 inches)[1]. Its centerline is aligned with that of the turbine rotor, and its position varies from 0.3175 to 4.1148 meters (12.5 to 162 inches) below the surface. The river subdomain is a half-cylinder with a diameter of 6.096 meters (240 inches). As with the first domain, the distance upstream of the turbine is 0.762 meters and the distance downstream is 3.81 meters. Figure 2a shows the total domain; Figure 2b displays the turbine inside the turbine subdomain.

[1] In the extreme cases where the turbine is only 0.3175 and 0.4191 meters (12.5 and 16.5 inches) below the surface, the turbine subdomain is limited to a diameter of 0.5842 and 0.6604 meters (23 and 26 inches), respectively.

The turbine is designed in ANSYS DesignModeler using BladeEditor, a plugin for creating and editing blade geometry. The design of the turbine blade is taken from [13], and it is the same for both parts of this study. The turbine is an axial turbine with two blades and a hydraulic diameter of 0.5334 meters (21 inches). Since the focus of this study is not the optimization of the turbine design, this simple model suffices for its purpose.

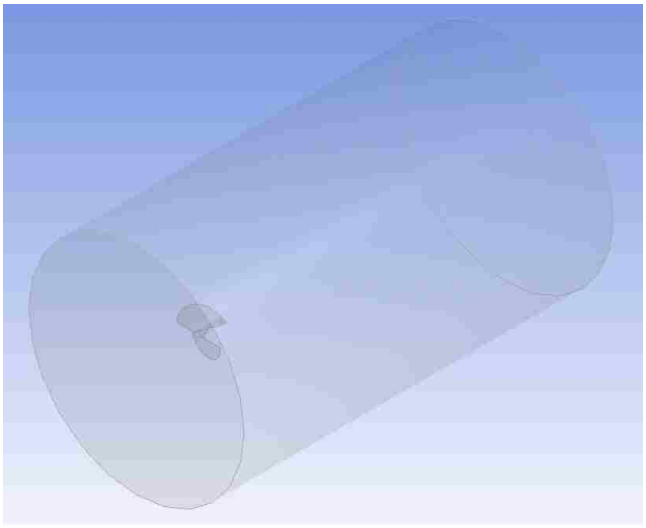

Figure 1: Duct Computational Domain

(a) (b)

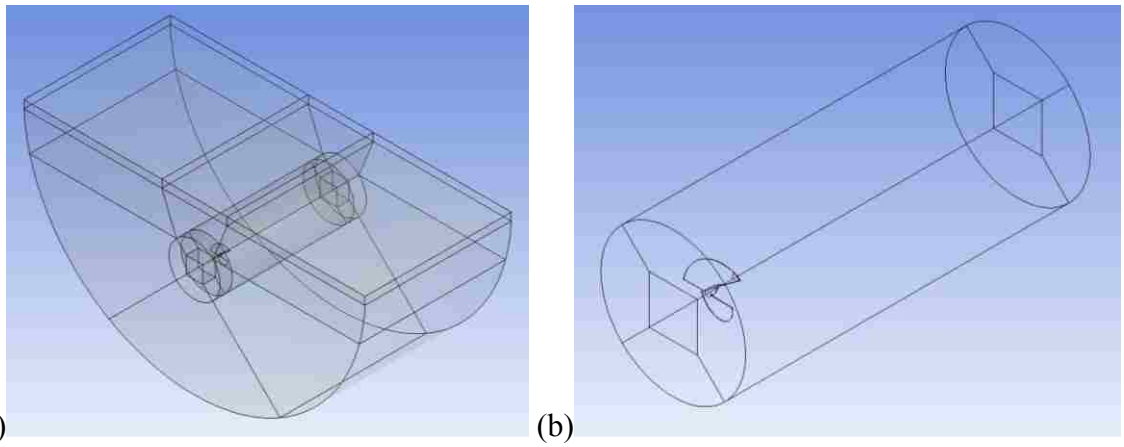

Figure 2: River Computational Domain: (a) Entire Domain (b) Turbine Subdomain

2.2 Meshing

The meshes for the first computational domain use tetrahedral and wedge elements. Two mesh sizes were employed for each simulation in order to determine convergence of the solution. These mesh sizes were a medium mesh of approximately 3.5 million elements and a fine mesh of approximately 5.5 million elements.

The meshes for the second domain use tetrahedral, hexahedral, and wedge elements. Here, only one mesh was used, a fine mesh containing approximately 5 million elements. The reasoning for this choice is explained later.

Figure 3 and Figure 4 show example meshes for the first and second domain, respectively. Figure 3a and Figure 4a portray the mesh for the entire domain. Figure 3b and Figure 4b depict cross-sectional views of the mesh; it can be seen in these views how the mesh element concentration varies throughout the domain, with a greater number of elements located near walls and the solid-liquid interface around the turbine. Figure 3c displays the mesh on the turbine blade, which is the same for both parts of this study.

(a)

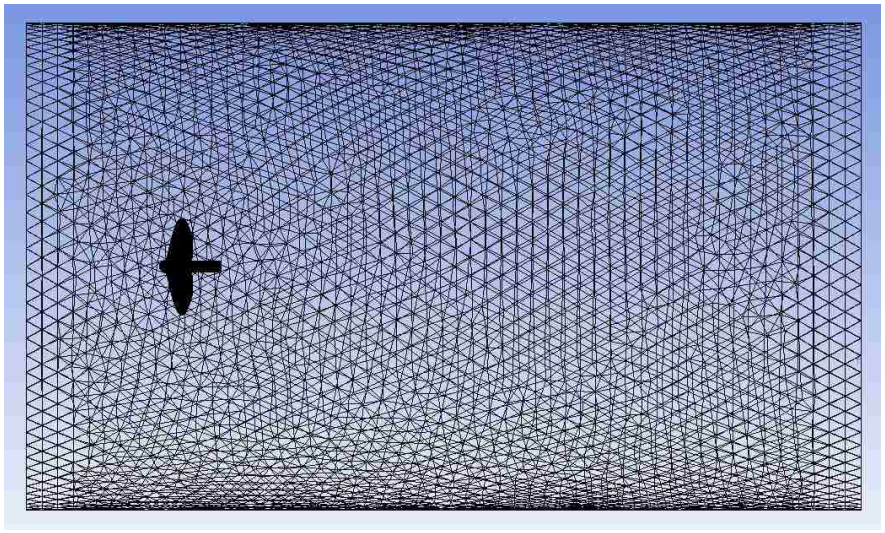

(b)

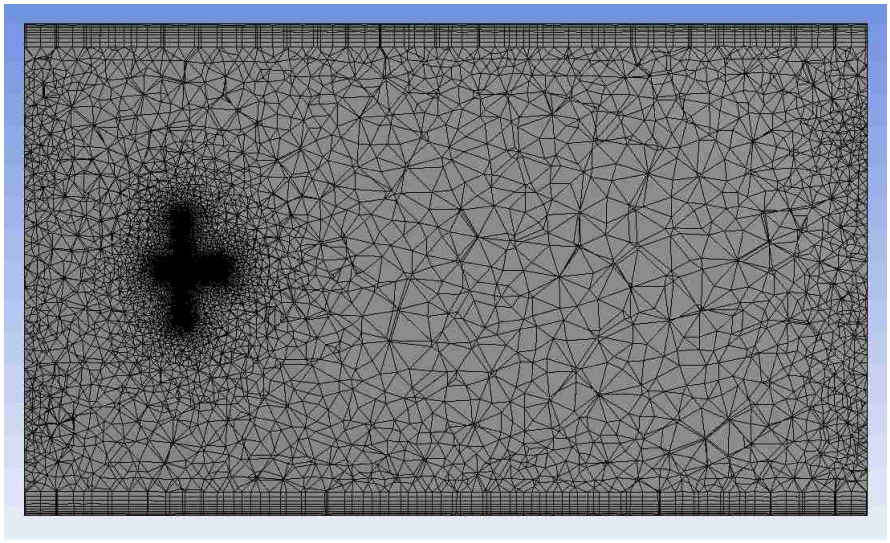

(c)

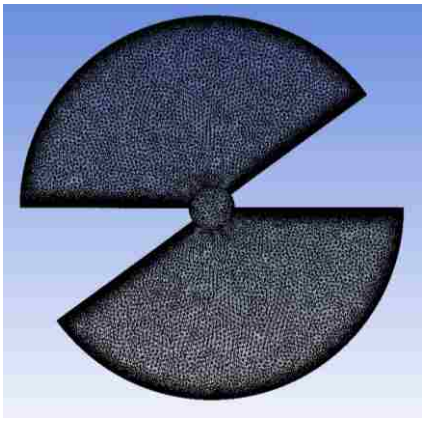

Figure 3: Duct Mesh: (a) Entire Domain (b) Cross-section (c) Turbine Blade

(a)

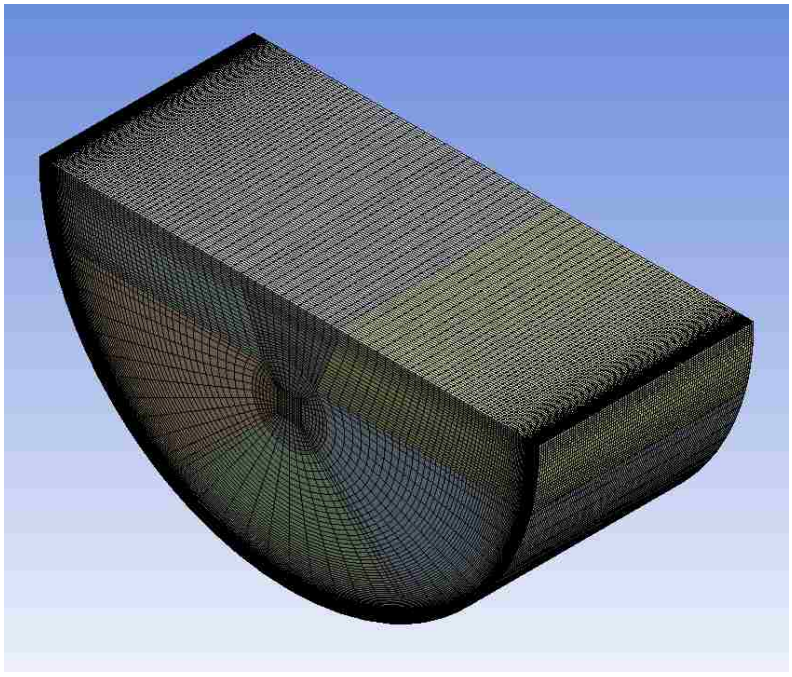

(b)

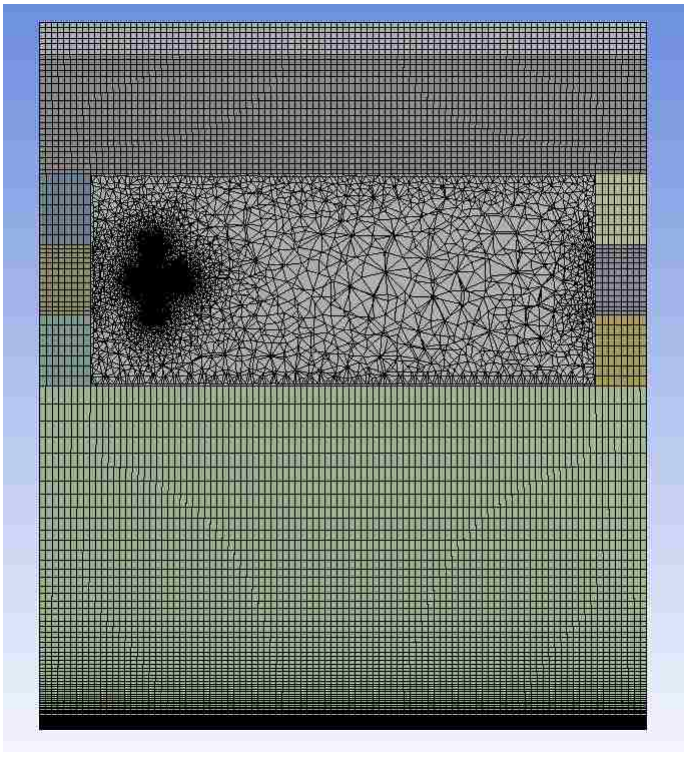

Figure 4: River Mesh: (a) Entire Domain (b) Cross-section

3. Models and Numerical Methods

3.1 Turbulence Model

In order to realistically model the water flow, turbulence needs to be accounted for. Several models exist for simulating turbulence, and the choice of model depends on certain aspects of the flow, such as Reynolds number and flow geometry.

The turbulence model used in this study is the Shear Stress Transport (SST) k-ω model, developed by Menter [14] in 1994. This model combines the standard k-ω model, which is accurate in regions close to walls, and the k-ε model, which is accurate in regions away from surfaces, making for an overall more accurate model [15]. The transport equations for the SST k-ω model are

$$\frac{\partial}{\partial t}(\rho k) + \frac{\partial}{\partial x_i}(\rho k u_i) = \frac{\partial}{\partial x_j}\left(\Gamma_k \frac{\partial k}{\partial x_j}\right) + \widetilde{G_k} - Y_k + S_k \tag{2}$$

$$\frac{\partial}{\partial t}(\rho \omega) + \frac{\partial}{\partial x_j}(\rho \omega u_j) = \frac{\partial}{\partial x_j}\left(\Gamma_\omega \frac{\partial \omega}{\partial x_j}\right) + G_\omega - Y_\omega + D_\omega + S_\omega \tag{3}$$

where

$$\Gamma_k = \mu + \frac{\mu_t}{\sigma_k} \qquad \Gamma_\omega = \mu + \frac{\mu_t}{\sigma_\omega} \tag{4}$$

$$\sigma_k = \frac{1}{F_1/\sigma_{k,1} + (1 - F_1)/\sigma_{k,2}} \qquad \sigma_\omega = \frac{1}{F_1/\sigma_{\omega,1} + (1 - F_1)/\sigma_{\omega,2}} \tag{5}$$

$$\mu_t = \frac{\rho k}{\omega}\frac{1}{\max\left[\frac{1}{\alpha^*}, \frac{SF_2}{a_1\omega}\right]} \qquad \alpha^* = \alpha^*_\infty\left(\frac{\alpha^*_0 + Re_t/R_k}{1 + Re_t/R_k}\right) \qquad \alpha^*_0 = \frac{\beta_i}{3} \tag{6}$$

$$\beta_i = F_1\beta_{i,1} + (1 - F_1)\beta_{i,2} \qquad Re_t = \frac{\rho k}{\mu\omega} \tag{7}$$

$$S = \sqrt{2S_{ij}S_{ij}} \qquad S_{ij} = \frac{1}{2}\left(\frac{\partial u_i}{\partial x_j} + \frac{\partial u_j}{\partial x_i}\right) \tag{8}$$

$$F_1 = \tanh(\Phi_1^4) \qquad \Phi_1 = \min\left[\max\left(\frac{\sqrt{k}}{0.09\omega y}, \frac{500\mu}{\rho y^2\omega}\right), \frac{4\rho k}{\sigma_{\omega,2}D^+_\omega y^2}\right] \tag{9}$$

$$D^+_\omega = \max\left[2\rho\frac{1}{\sigma_{\omega,2}}\frac{1}{\omega}\frac{\partial k}{\partial x_j}\frac{\partial \omega}{\partial x_j}, 10^{-10}\right] \tag{10}$$

$$F_2 = \tanh(\Phi_2^2) \qquad \Phi_2 = \max\left[2\frac{\sqrt{k}}{0.09\omega y}, \frac{500\mu}{\rho y^2\omega}\right] \tag{11}$$

$$D_\omega = 2(1 - F_1)\rho\frac{1}{\omega\sigma_{\omega,2}}\frac{\partial k}{\partial x_j}\frac{\partial \omega}{\partial x_j} \tag{12}$$

$$\widetilde{G_k} = \min(G_k, 10\rho\beta^* k\omega) \qquad G_k = -\rho\overline{u'_i u'_j}\frac{\partial u_j}{\partial x_i} \tag{13}$$

$$\beta^* = \beta^*_i[1 + \zeta^* F(M_t)] \qquad \beta^*_i = \beta^*_\infty\left[\frac{4/15 + \left(Re_t/R_\beta\right)^4}{1 + \left(Re_t/R_\beta\right)^4}\right] \tag{14}$$

$$F(M_t) = \begin{cases} 0, & M_t \le M_{t0} \\ M_t^2 - M_{t0}^2, & M_t > M_{t0} \end{cases} \qquad M_t^2 \equiv \frac{2k}{a^2} \tag{15}$$

$$G_\omega = \frac{\alpha}{\nu_t}G_k \qquad \alpha = \frac{\alpha_\infty}{\alpha^*}\left(\frac{\alpha_0 + Re_t/R_\omega}{1 + Re_t/R_\omega}\right) \qquad \alpha_\infty = F_1\alpha_{\infty,1} + (1 - F_1)\alpha_{\infty,2} \tag{16}$$

$$\alpha_{\infty,1} = \frac{\beta_{i,1}}{\beta^*_\infty} - \frac{\kappa^2}{\sigma_{\omega,1}\sqrt{\beta^*_\infty}} \qquad \alpha_{\infty,2} = \frac{\beta_{i,2}}{\beta^*_\infty} - \frac{\kappa^2}{\sigma_{\omega,2}\sqrt{\beta^*_\infty}} \tag{17}$$

$$Y_k = \rho\beta^* k\omega \qquad Y_\omega = \rho\beta\omega^2 \tag{18}$$

$$a_1 = 0.31, \quad \sigma_{k,1} = 1.176, \quad \sigma_{\omega,1} = 2.0, \quad \sigma_{k,2} = 1.0, \quad \sigma_{\omega,2} = 1.168$$

$$\alpha^*_\infty = 1, \quad R_k = 6, \quad \beta_{i,1} = 0.075, \quad \beta_{i,2} = 0.0828, \quad \zeta^* = 1.5$$

$$\beta^*_\infty = 0.09, \quad R_\beta = 8, \quad M_{t0} = 0.25, \quad \alpha_0 = \frac{1}{9}, \quad R_\omega = 2.95, \quad \kappa = 0.41$$

In the above equations: t is time; ρ is the density; k is the turbulence kinetic energy; ω is the specific dissipation rate; x is a position vector; u is a velocity vector; Γ_k and Γ_ω are the effective diffusivity of k and ω, respectively; μ is the dynamic viscosity; σ_k and σ_ω are the turbulent Prandtl numbers for k and ω, respectively; μ_t is the turbulent dynamic viscosity; F_1 and F_2 are blending functions; α^* is a correction coefficient; Re_t is the turbulent Reynolds number; S is the magnitude of the mean rate-of-strain tensor, S_{ij}; y is the distance to the next surface; D^+_ω is the positive portion of the cross-diffusion term, D_ω; $\widetilde{G_k}$ and G_k are the generation of k due to mean velocity gradients; M_t is the turbulent Mach number; a is the speed of sound; G_ω is the generation of ω; ν_t is the turbulent kinematic viscosity; Y_k and Y_ω are the dissipation due to turbulence of k and ω, respectively; S_k and S_ω are user-defined source terms; the sub scripts i, j, and k denote vector integers; α^*_0, β_i, Φ_1, Φ_2, β^*, β^*_i, α, α_∞, $\alpha_{\infty,1}$, and $\alpha_{\infty,2}$ are parametric constants; and the remaining symbols are constants, defined above.

3.2 Rotating Reference Frame

The rotating turbine blade makes this problem transient in nature; however, instead of rotating the blade, the reference frame in the region near the blade can be rotated in the simulation. This modeling option, which calculates the solution relative to the moving reference frame, allows the problem to be treated as steady. However, in order to solve the problem in this manner, the governing equations must be modified. The modified equations for conservation of mass and momentum are, respectively,

$$\frac{\partial \rho}{\partial t} + \nabla \cdot \rho \bar{v}_r = 0 \tag{19}$$

$$\frac{\partial}{\partial t}(\rho \bar{v}_r) + \nabla \cdot (\rho \bar{v}_r \bar{v}_r) + \rho(2\bar{\omega} \times \bar{v}_r + \bar{\omega} \times \bar{\omega} \times \bar{r}) = -\nabla P + \nabla \cdot \bar{\bar{\tau}}_r + \bar{F} \tag{20}$$

where ∇ is the vector differential operator; $\bar{v}_r$ is the relative velocity vector; $\bar{\omega}$ is the angular velocity vector; $\bar{r}$ is the position vector from the origin of the moving frame to an arbitrary point in the computational domain; P is the pressure; $\bar{\bar{\tau}}_r$ is the viscous stress tensor; and $\bar{F}$ is the external force vector per unit length. In Equation (20), the last two terms on the left-hand side account for Coriolis and centrifugal accelerations.

3.3 Boundary Conditions

Appropriate boundary conditions need to be set in order to obtain an accurate solution. The velocity profile at the inlet of the computational domain is assumed to be fully-developed. The equations governing this profile are as follows:

$$\frac{\bar{u}}{U} = \left(1 - \frac{r}{R}\right)^{1/n} \tag{21}$$

$$n = -1.7 + 1.8 \ln Re_U, \tag{22}$$

where $\bar{u}$ is the average local velocity; U is the maximum velocity; r is the local radius; R is the radius of the channel; n is a parametric constant; and Re_U is Reynolds number based on the maximum velocity and the channel diameter.

Turbulence parameters, namely, turbulence intensity and hydraulic diameter, are defined at the inlet and outlet. Turbulence intensity, I, changes according to the relation $I = 0.16 {Re_{D_H}}^{-1/8}$, where Re_{D_H} is Reynolds number based on the hydraulic diameter. Hydraulic diameter, D_H, is set equal to the channel diameter, thus varying in value among simulations. FLUENT uses these two parameters to calculate turbulence kinetic energy (k) and specific dissipation rate (ω) as follows:

$$k = \frac{3}{2}\left(u_{avg} I\right)^2 \tag{23}$$

$$\omega = \frac{k^{1/2}}{C_\mu^{1/4} l} \tag{24}$$

where u_{avg} is the average flow velocity; C_μ is a specified empirical constant; and $l = 0.07 D_H$ is the turbulence length scale.

The turbine is set as a moving wall with zero angular velocity relative to the frame of reference in the region near the turbine, which is set to rotate at a rate of 250 RPM (or approximately 26.18 rad/s). This setup thus mimics the rotating motion of the

turbine, as discussed above. For the circular duct domain, the duct is set as a moving wall with zero absolute rotational velocity; this condition ensures that the duct does not rotate with the reference frame. For the river domain, the shear along the free (top) surface of the river is set to zero. In both cases, the pressure at the outlet is set to zero.

4. Results and Discussion

The following results have been obtained using an average inlet flow velocity of 3.5 m/s and a blade rotation rate of 250 RPM. These parameters correspond to a tip-speed ratio (TSR) of about 2, where tip-speed ratio is the ratio of the tangential velocity of the outermost edge of the blade to the average flow velocity.

The results for both parts of this study are presented using the dimensionless parameter coefficient of performance, C_p, which is defined as

$$C_p = \frac{P_E}{P_A} = \frac{T\omega_f}{\frac{1}{2}\rho A_t \left(u_{avg}\right)^3} \tag{25}$$

where P_E is the power extracted from the turbine; P_A is the potential power available in the flow field; T is the calculated torque on the turbine; ω_f is the angular frequency of the turbine; ρ is the density of the fluid; A_t is the cross-sectional area swept out by the turbine; and u_{avg} is the average flow velocity.

4.1 Blockage Ratio Results

Coefficient of performance as a function of blockage ratio is shown in Figure 5. At low values of blockage ratio, the coefficient of performance appears to reach an asymptotic value of about 0.5. In fact, not much variation is seen for blockage ratios less than about 0.4. This would suggest that, regardless of the size of the channel, a hydrokinetic turbine will extract at least fifty percent of the available energy. However,

the value of this lower limit may change for different channel flow velocities and turbine rotation rates, but such results are outside the interest of this particular study.

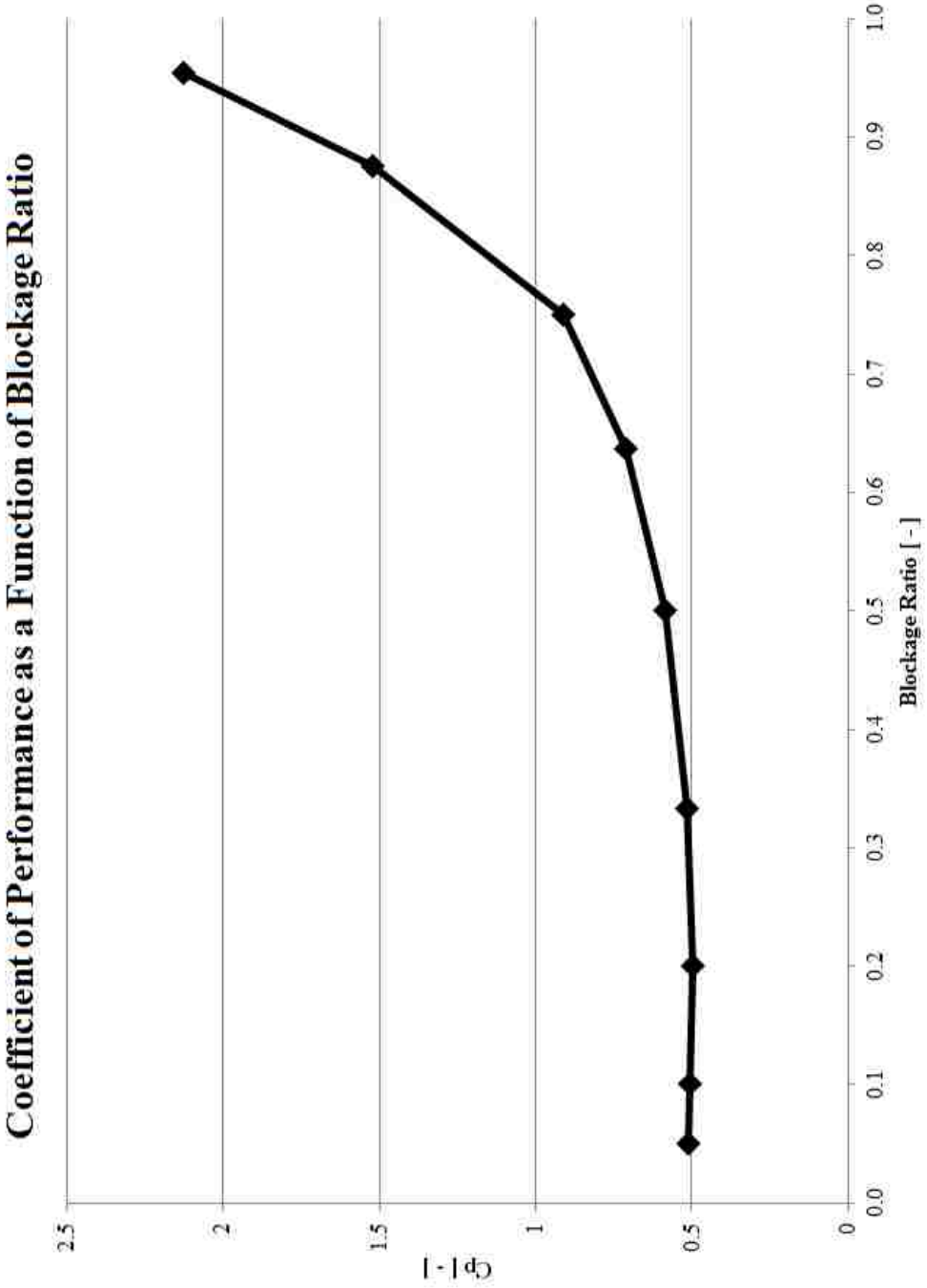

Figure 5: Coefficient of Performance as a Function of Blockage Ratio

These results are of particular importance to those who are attempting to optimize other performance characteristics of hydrokinetic turbines. Such individuals should run models with blockage ratios less than 0.4 (or even less than 0.3 to be safe) to ensure that their results are independent of the effects of blockage ratio.

As the blockage ratio increases above 0.4, the coefficient of performance begins to increase rapidly. Graphically, it appears that a vertical asymptote exists as the blockage ratio approaches 1. Whereas infinite power output does not make sense physically, such results agree mathematically with [11]. Regardless, the results contained in Figure 5 show that the coefficient of performance increases with increasing blockage ratio for a single hydrokinetic turbine. Therefore, anyone seeking to set up a hydrokinetic turbine should do so in a location where the blockage ratio is as large as reasonably possible.

As regards coefficient of performance values greater than 1 in the above results, these values occur for high blockage ratios (approximately greater than 0.8) where the distance between the turbine and duct wall is rather small. In these cases, the low clearance forces water from the region near the wall through the turbine, and because the available power is calculated only from the water occupying the same cross-sectional area as the turbine, coefficient of performance values greater than 1 are possible.

Looking at streamlines can help in understanding this point. Figure 6 displays images of streamlines from ANSYS CFD-Post for a few values of blockage ratio. At lower values of blockage ratio, the duct is far from the turbine blade, so the streamlines

are unrestricted. However, at higher values of blockage ratio, the low clearance between the duct and blade restricts the streamlines, and more water is forced through the turbine.

Figure 7 more thoroughly compares this study's numerical results with the analytical results of [11]. The values from this study lie beneath the proposed maximum coefficient of performance curve. Regarding this drop in the expected coefficient of performance, Garrett and Cummins state in their work, "If it is assumed … that lateral mixing of the wake and free stream downstream of the turbine restores the flow to a uniform state, then some energy is dissipated in this mixing…." Said assumption is made in this study in order to ensure that the distance from the turbine to the outlet of the computational domain does not affect the results.

Figure 8 shows total pressure contours for multiple blockage ratio values. Not much difference in the contours can be seen between values of 0.05 and 0.50, though the onset of higher total pressure begins to appear along the leading edge at 0.50. As the blockage ratio climbs to 0.875 and 0.955, total pressure increases along the outer edge of the blades and decreases in the near-rotor region.

Velocity contours are displayed in Figure 9 for multiple values of blockage ratio. The velocity contours for values from 0.05 to 0.33 remain approximately the same, with the highest velocity values appearing at the outer edge of the turbine blade. As the blockage ratio reaches 0.50, areas of higher velocity begin to appear off the trailing edge of the blade. At values of 0.875 and 0.955, regions of high velocity are present immediately downstream of the blade.

Figure 10 displays vorticity contours for multiple values of blockage ratio. For each blockage ratio value, contours are shown at four positions along the flow: 0.0508 meters (2 inches) upstream, 0.0762 meters (3 inches) downstream, 0.2286 meters (9 inches) downstream, and 0.4572 meters (18 inches) downstream, measured from the leading edge of the blade. Regions of high vorticity occur along the surface of the blade and immediately downstream of the tip of the blade for all values of blockage ratio. Above values of 0.75, larger regions of high vorticity develop immediately downstream of the blade midway between the rotor and the blade tip.

Figure 11 shows vortex ropes for different values of blockage ratio, demonstrating the swirling nature of the flow downstream of the turbine. Not much change is seen below values of 0.50, but as the blockage ratio increases above 0.50, more greatly confining the flow, vortex strength increases as expected. As can been seen in Figure 11f, downstream vortices become very strong as the blockage ratio approaches 1.

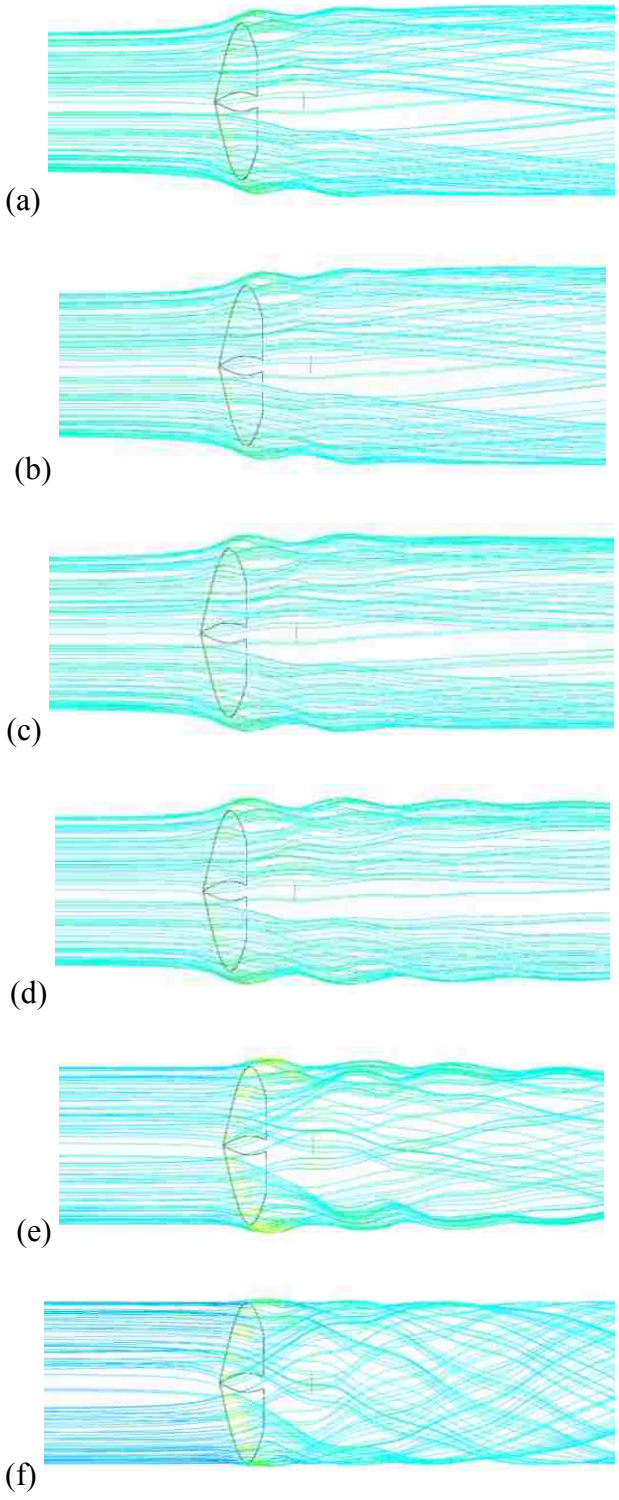

$B =$ (a) 0.5, (b) 0.20, (c) 0.50, (d) 0.636, (e) 0.875, (f) 0.955

Figure 6: Streamlines for Various Values of Blockage Ratio

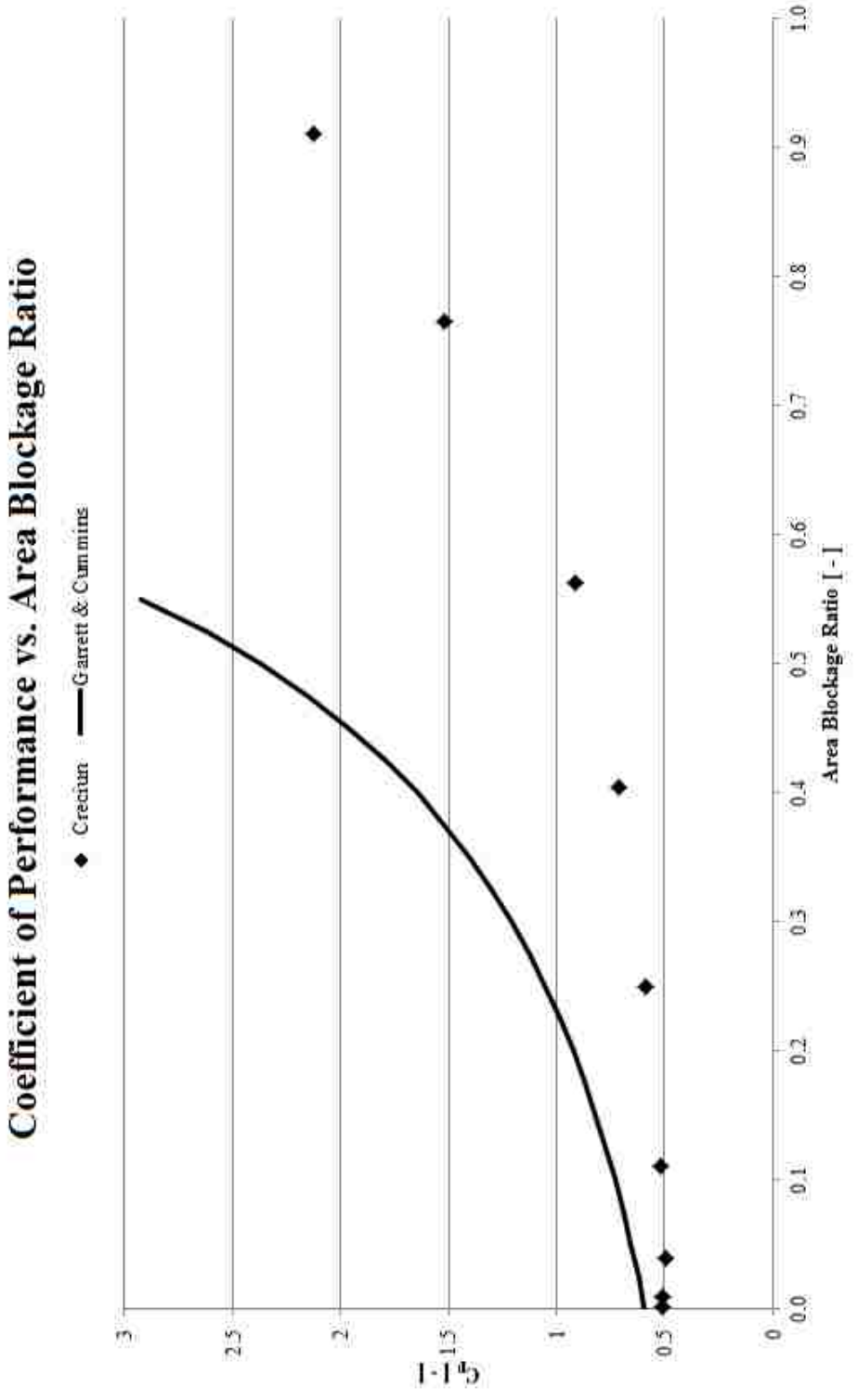

Figure 7: Comparison of Results with Garrett & Cummins 2007 Study

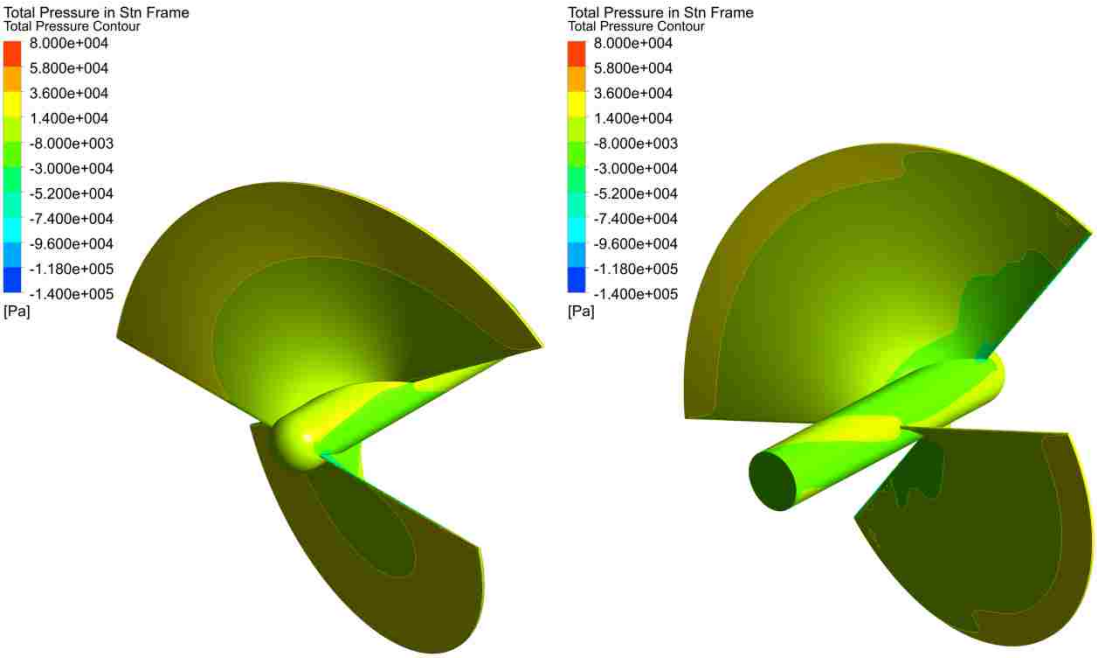
Total Pressure in Stn Frame
Total Pressure Contour
8.000e+004
5.800e+004
3.600e+004
1.400e+004
-8.000e+003
-3.000e+004
-5.200e+004
-7.400e+004
-9.600e+004
-1.180e+005
-1.400e+005
[Pa]
Total Pressure in Stn Frame
Total Pressure Contour
8.000e+004
5.800e+004
3.600e+004
1.400e+004
-8.000e+003
-3.000e+004
-5.200e+004
-7.400e+004
-9.600e+004
-1.180e+005
-1.400e+005
[Pa]

(a)

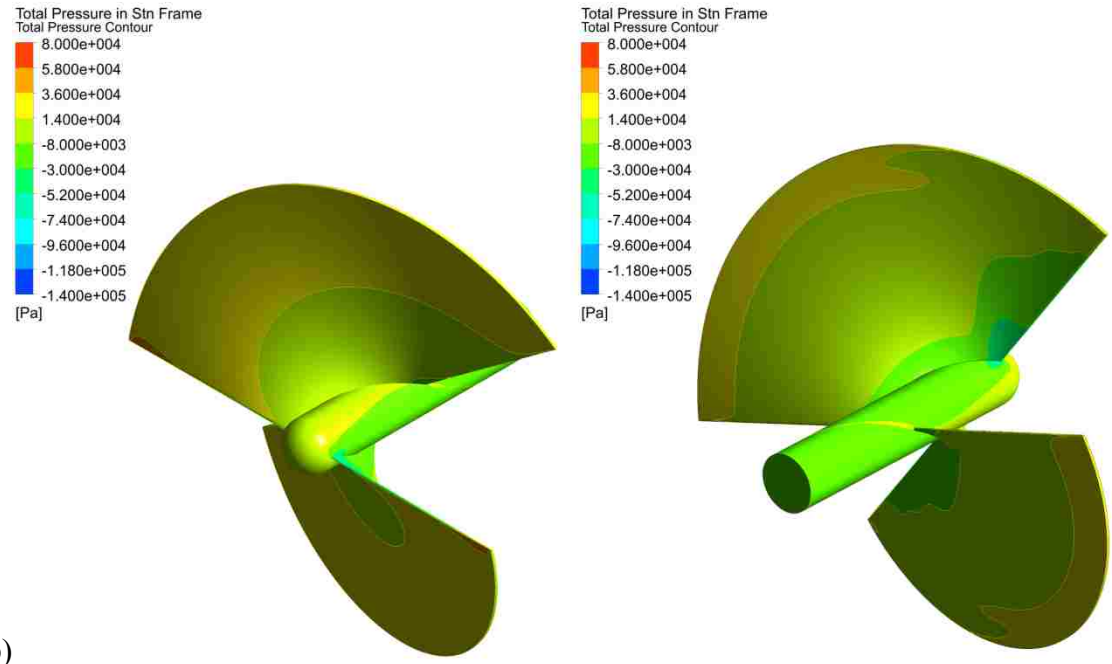
Total Pressure in Stn Frame
Total Pressure Contour
8.000e+004
5.800e+004
3.600e+004
1.400e+004
-8.000e+003
-3.000e+004
-5.200e+004
-7.400e+004
-9.600e+004
-1.180e+005
-1.400e+005
[Pa]
Total Pressure in Stn Frame
Total Pressure Contour
8.000e+004
5.800e+004
3.600e+004
1.400e+004
-8.000e+003
-3.000e+004
-5.200e+004
-7.400e+004
-9.600e+004
-1.180e+005
-1.400e+005
[Pa]

(b)

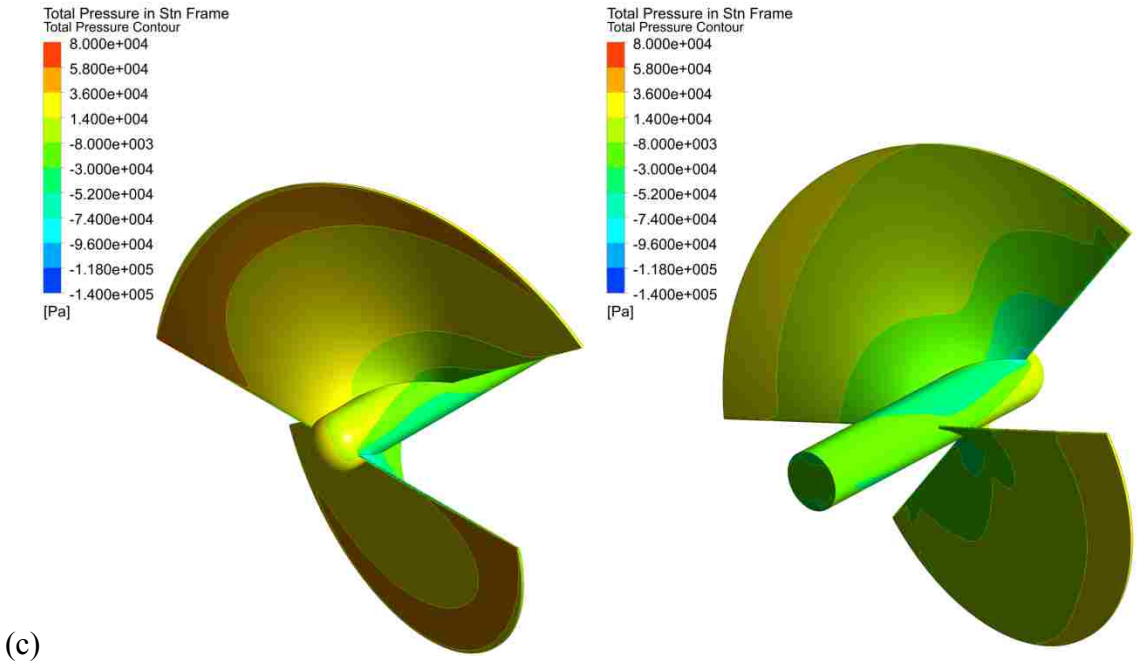

(c)

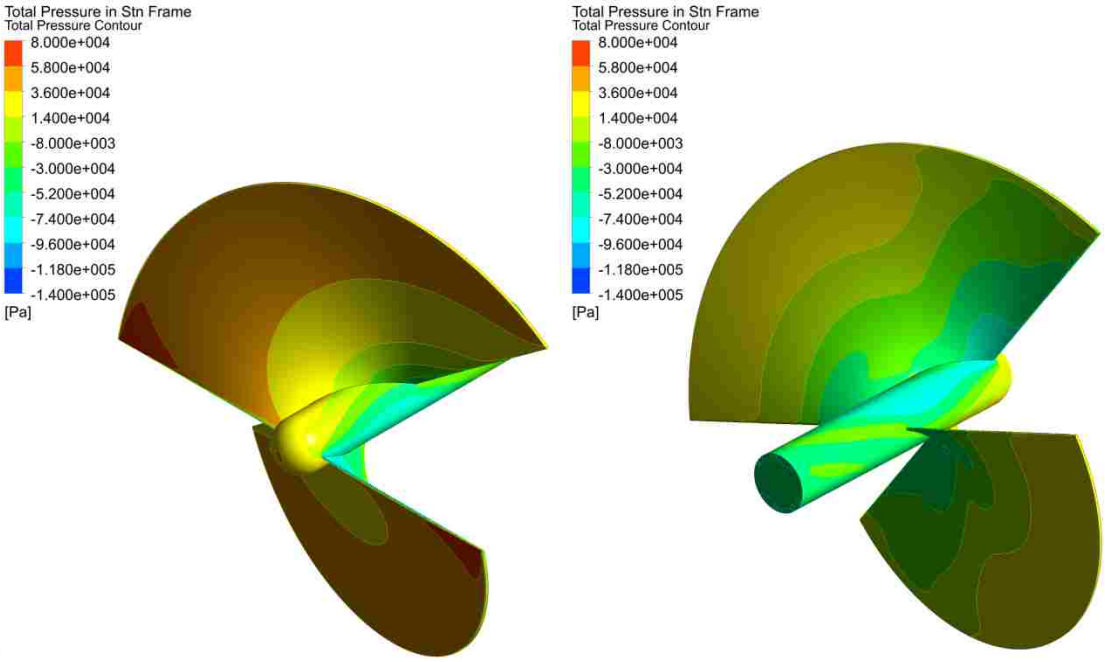

(d)

B = (a) 0.05, (b) 0.50, (c) 0.875, (d) 0.955

Figure 8: Turbine Total Pressure Contours for Various Values of Blockage Ratio

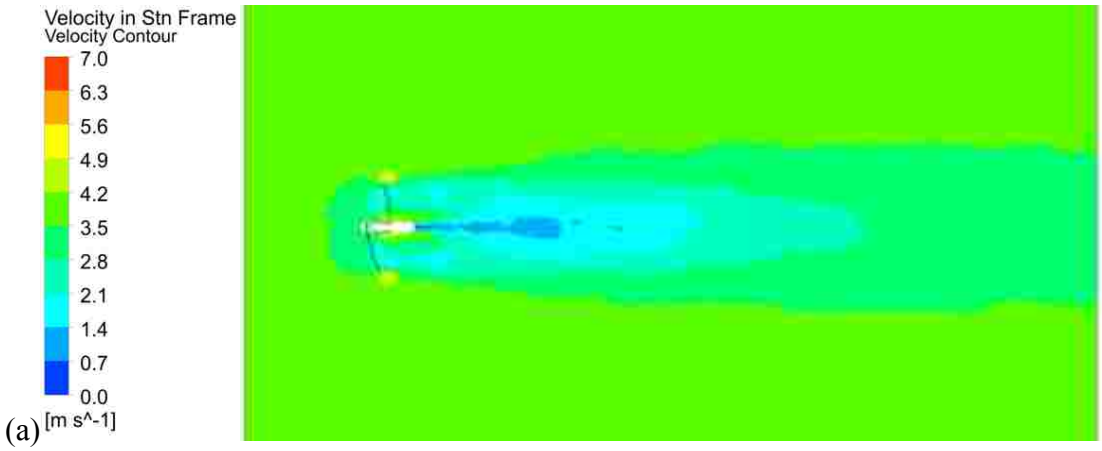
Velocity in Stn Frame
Velocity Contour
7.0
6.3
5.6
4.9
4.2
3.5
2.8
2.1
1.4
0.7
0.0
[m s^-1]

(a)

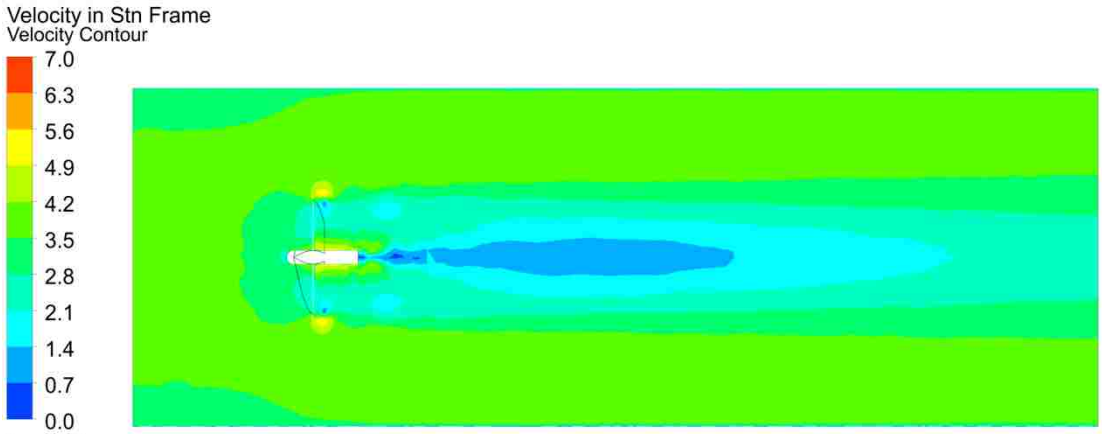
Velocity in Stn Frame
Velocity Contour
7.0
6.3
5.6
4.9
4.2
3.5
2.8
2.1
1.4
0.7
0.0
[m s^-1]

(b)

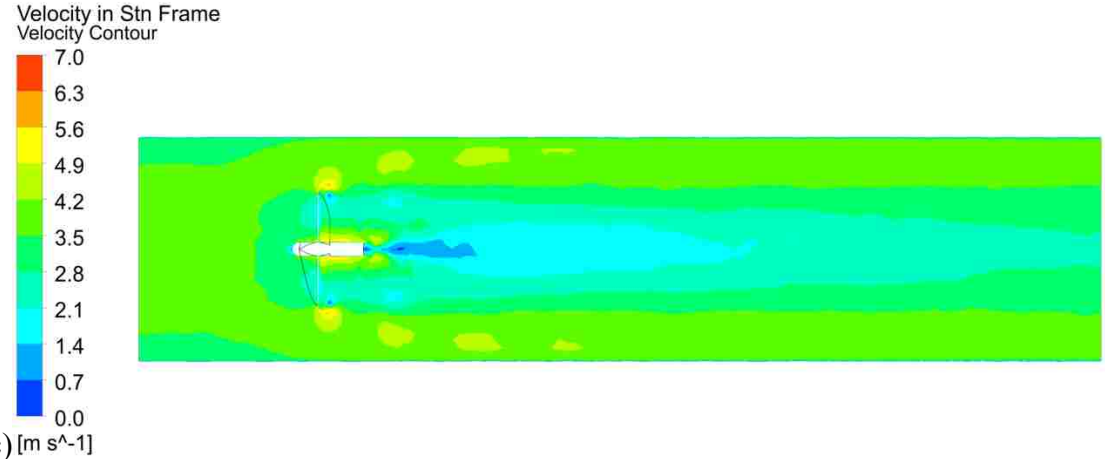
Velocity in Stn Frame
Velocity Contour
7.0
6.3
5.6
4.9
4.2
3.5
2.8
2.1
1.4
0.7
0.0
[m s^-1]

(c)

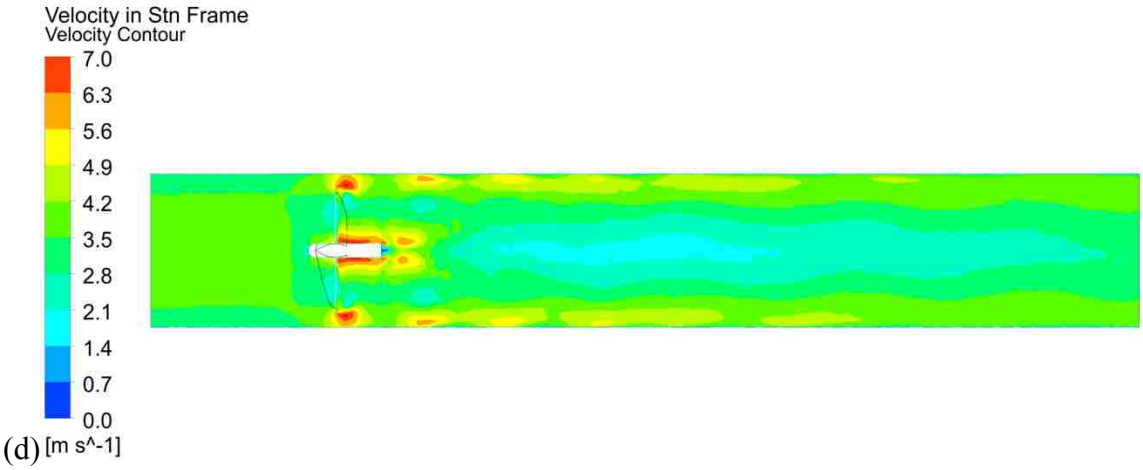

(d)

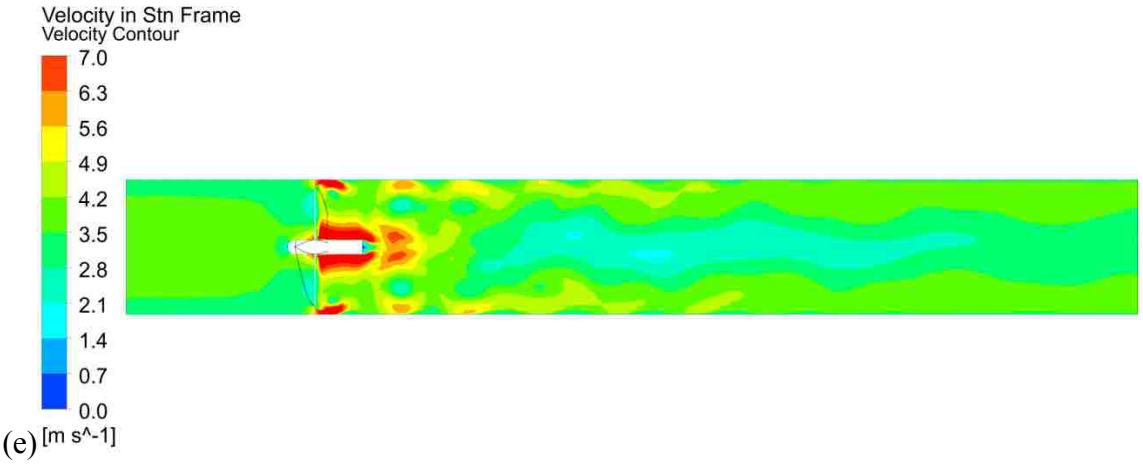

(e)

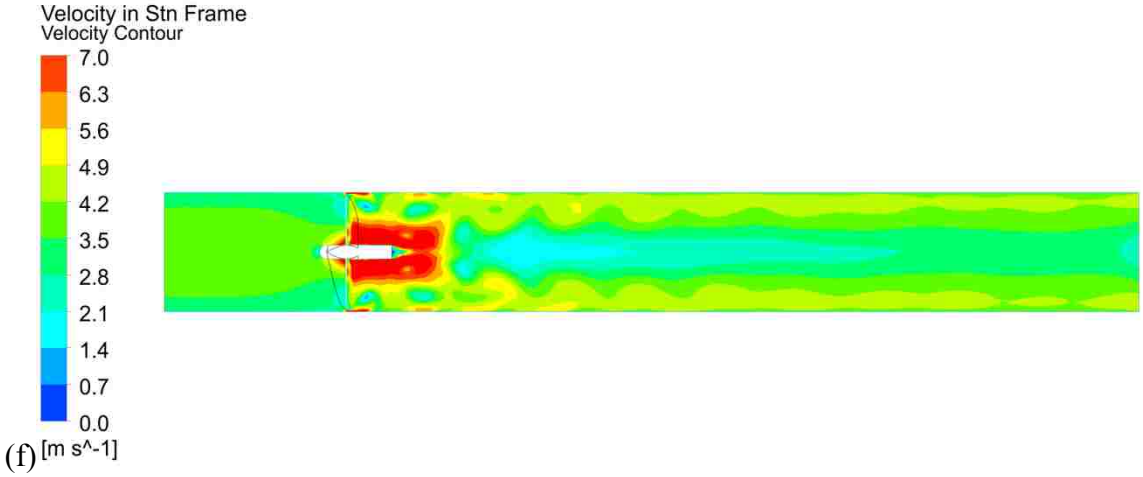

(f)

B = (a) 0.05, (b) 0.33, (c) 0.50, (d) 0.75, (e) 0.875, (f) 0.955

Figure 9: Velocity Contours for Various Values of Blockage Ratio

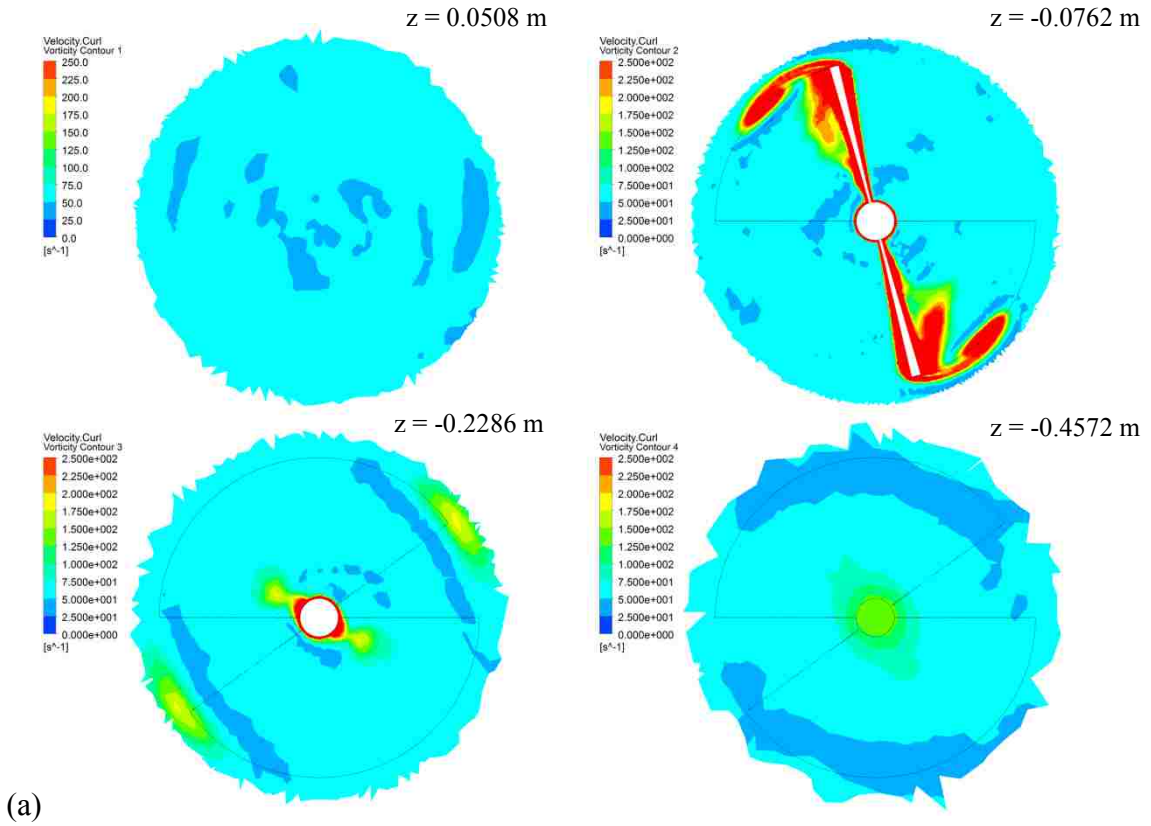
z = 0.0508 m
z = -0.0762 m
z = -0.2286 m
z = -0.4572 m
Velocity.Curl
Vorticity Contour 1
250.0
225.0
200.0
175.0
150.0
125.0
100.0
75.0
50.0
25.0
0.0
[s^-1]
Velocity.Curl
Vorticity Contour 2
2.500e+002
2.250e+002
2.000e+002
1.750e+002
1.500e+002
1.250e+002
1.000e+002
7.500e+001
5.000e+001
2.500e+001
0.000e+000
[s^-1]
Velocity.Curl
Vorticity Contour 3
2.500e+002
2.250e+002
2.000e+002
1.750e+002
1.500e+002
1.250e+002
1.000e+002
7.500e+001
5.000e+001
2.500e+001
0.000e+000
[s^-1]
Velocity.Curl
Vorticity Contour 4
2.500e+002
2.250e+002
2.000e+002
1.750e+002
1.500e+002
1.250e+002
1.000e+002
7.500e+001
5.000e+001
2.500e+001
0.000e+000
[s^-1]

(a)

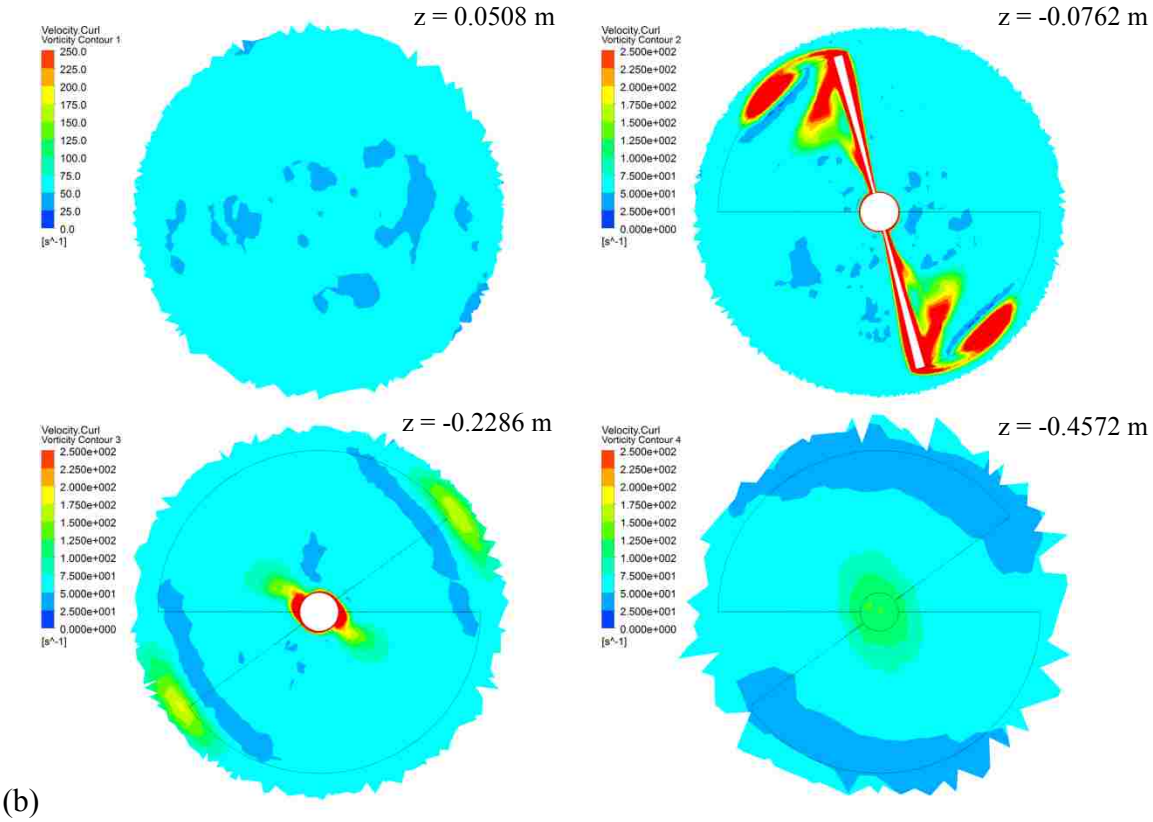
z = 0.0508 m
z = -0.0762 m
z = -0.2286 m
z = -0.4572 m
Velocity.Curl
Vorticity Contour 1
250.0
225.0
200.0
175.0
150.0
125.0
100.0
75.0
50.0
25.0
0.0
[s^-1]
Velocity.Curl
Vorticity Contour 2
2.500e+002
2.250e+002
2.000e+002
1.750e+002
1.500e+002
1.250e+002
1.000e+002
7.500e+001
5.000e+001
2.500e+001
0.000e+000
[s^-1]
Velocity.Curl
Vorticity Contour 3
2.500e+002
2.250e+002
2.000e+002
1.750e+002
1.500e+002
1.250e+002
1.000e+002
7.500e+001
5.000e+001
2.500e+001
0.000e+000
[s^-1]
Velocity.Curl
Vorticity Contour 4
2.500e+002
2.250e+002
2.000e+002
1.750e+002
1.500e+002
1.250e+002
1.000e+002
7.500e+001
5.000e+001
2.500e+001
0.000e+000
[s^-1]

(b)

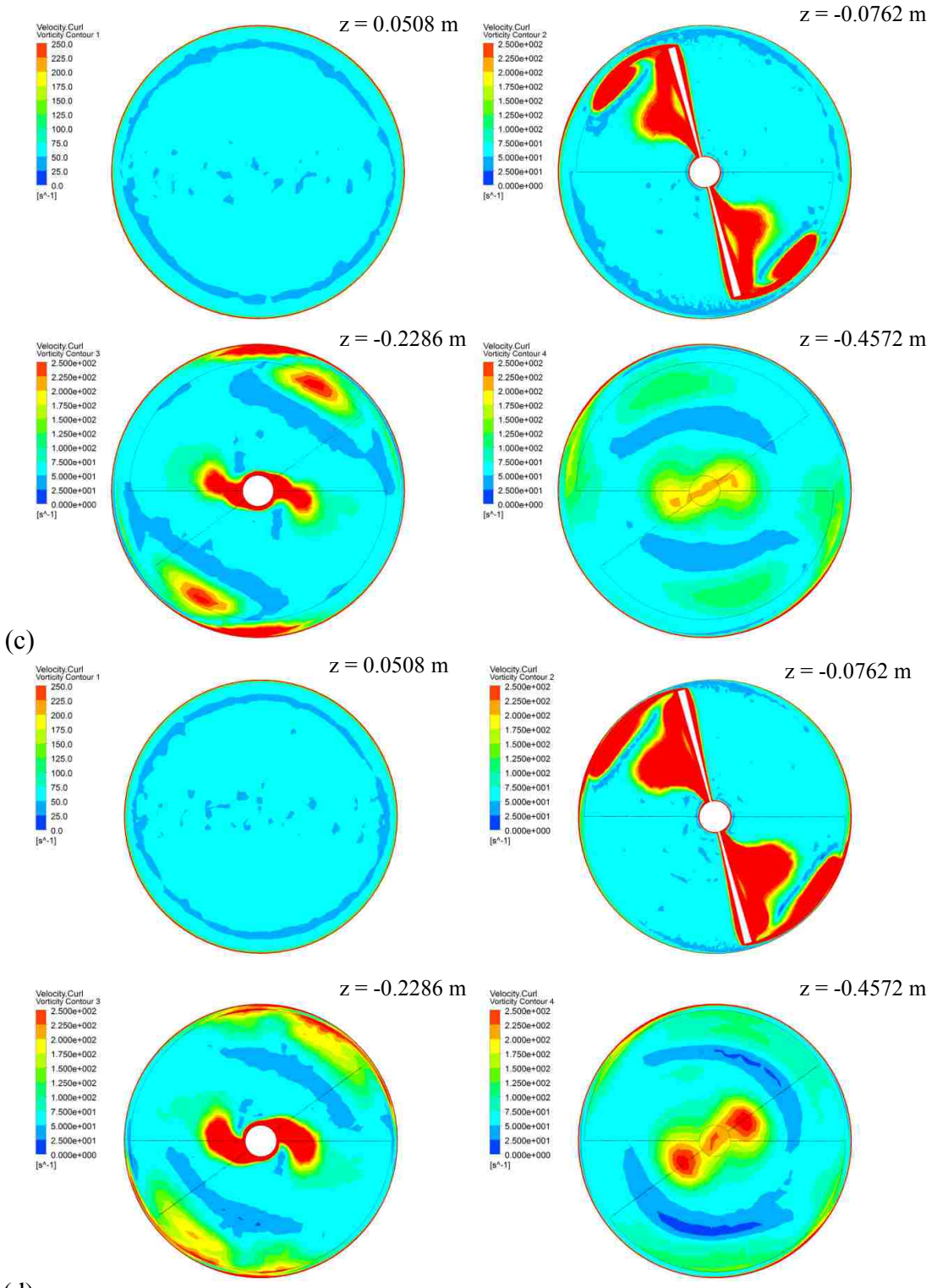

B = (a) 0.05, (b) 0.636, (c) 0.875, (d) 0.955

Figure 10: Vorticity Contours for Various Values of Blockage Ratio

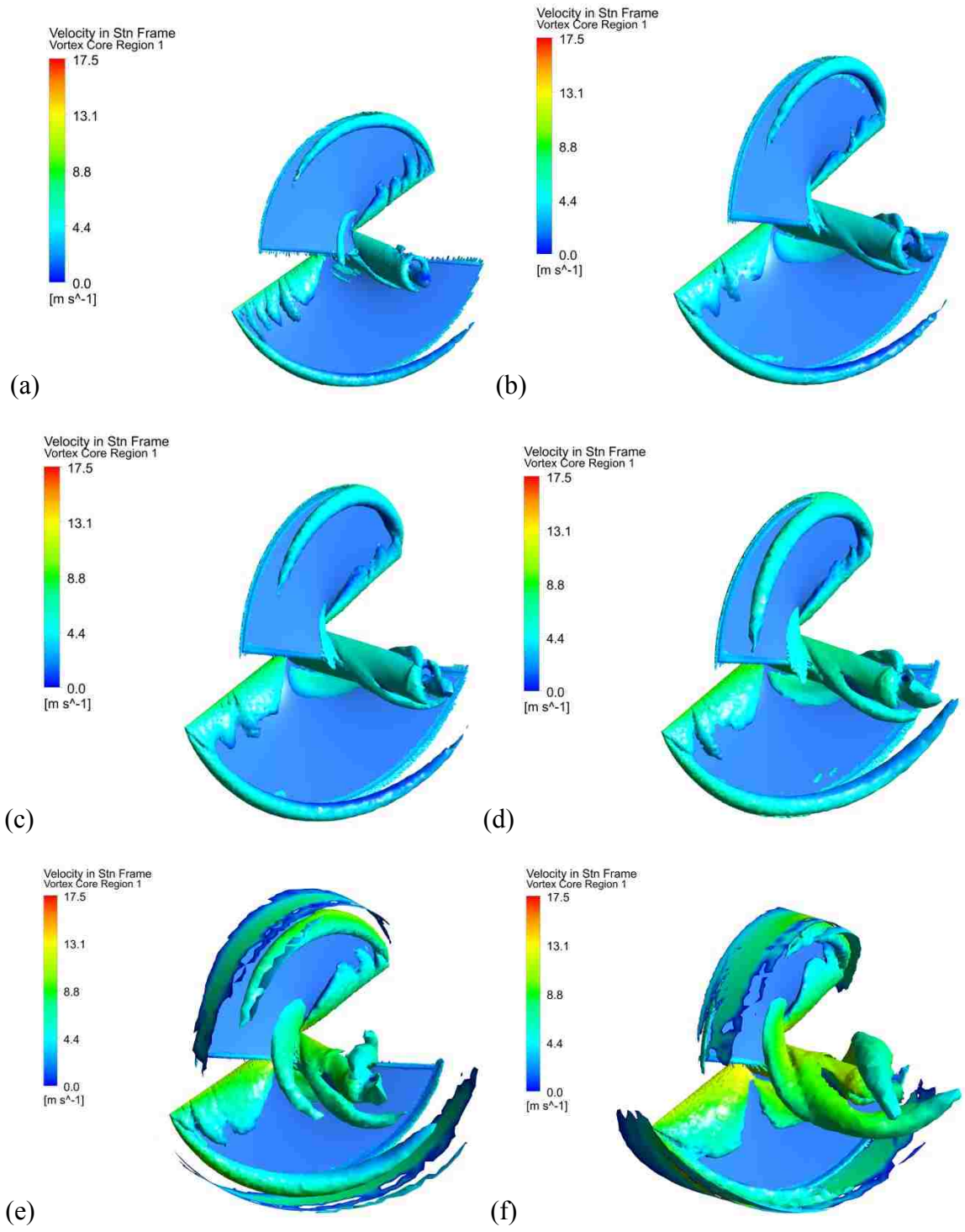

B = (a) 0.05, (b) 0.20, (c) 0.50, (d) 0.75, (e) 0.875, (f) 0.955

Figure 11: Vortex Ropes for Various Values of Blockage Ratio

4.2 Surface Effect Results

Coefficient of performance as a function of turbine depth (measured from the center of the turbine rotor) is shown in Figure 12. It appears that the distance of the turbine below the free surface does not have much effect on turbine performance for distances greater than 0.4191 meters (16.5 inches), but for distances less than 0.4191 meters, turbine performance is shown to increase. This increase is likely linked to the maximum flow velocity occurring at the free surface. When the turbine is located sufficiently close to the free surface, whose zero-shear boundary condition does not slow down the flow speed, the flow through the turbine approaches the maximum possible velocity, and the corresponding power output is greater than that for other turbine depths.

Figure 13 shows streamlines for different values of turbine depth. For most values, the streamlines remain unchanged. It is only when the turbine is placed very close to the free surface (see Figure 13d) that the streamlines become constrained. Figure 14 displays pressure contours on the turbine blade. Again, little change is seen among different values of turbine depth except for when the turbine is very close to the free surface. Velocity contours, shown in Figure 15, also follow this pattern: not much variation is seen until the turbine is at a depth of 0.4191 meters, where the downstream wake of the turbine gets longer and the velocity near the tip of the blade gets higher. Vorticity contours and vorticy ropes, displayed in Figure 16 and Figure 17, respectively, further confirm this observation.

However, it is possible that these results are not accurate. The computational domain for this part of the study is limited to a riverbed, but a more accurate domain would include air above the river. In the current model, the free surface is given the simple boundary condition of a wall without shear, but the model including air would allow for the water to move into the air region and vice versa. Such a model would be significantly more complex than the one used in this study since the flow would become two-phase. The use of a finer mesh may also allow for more accurate results, but an appropriately-sized mesh may require as many as 10 million elements, which is beyond the capacity of the computing power available for this study.

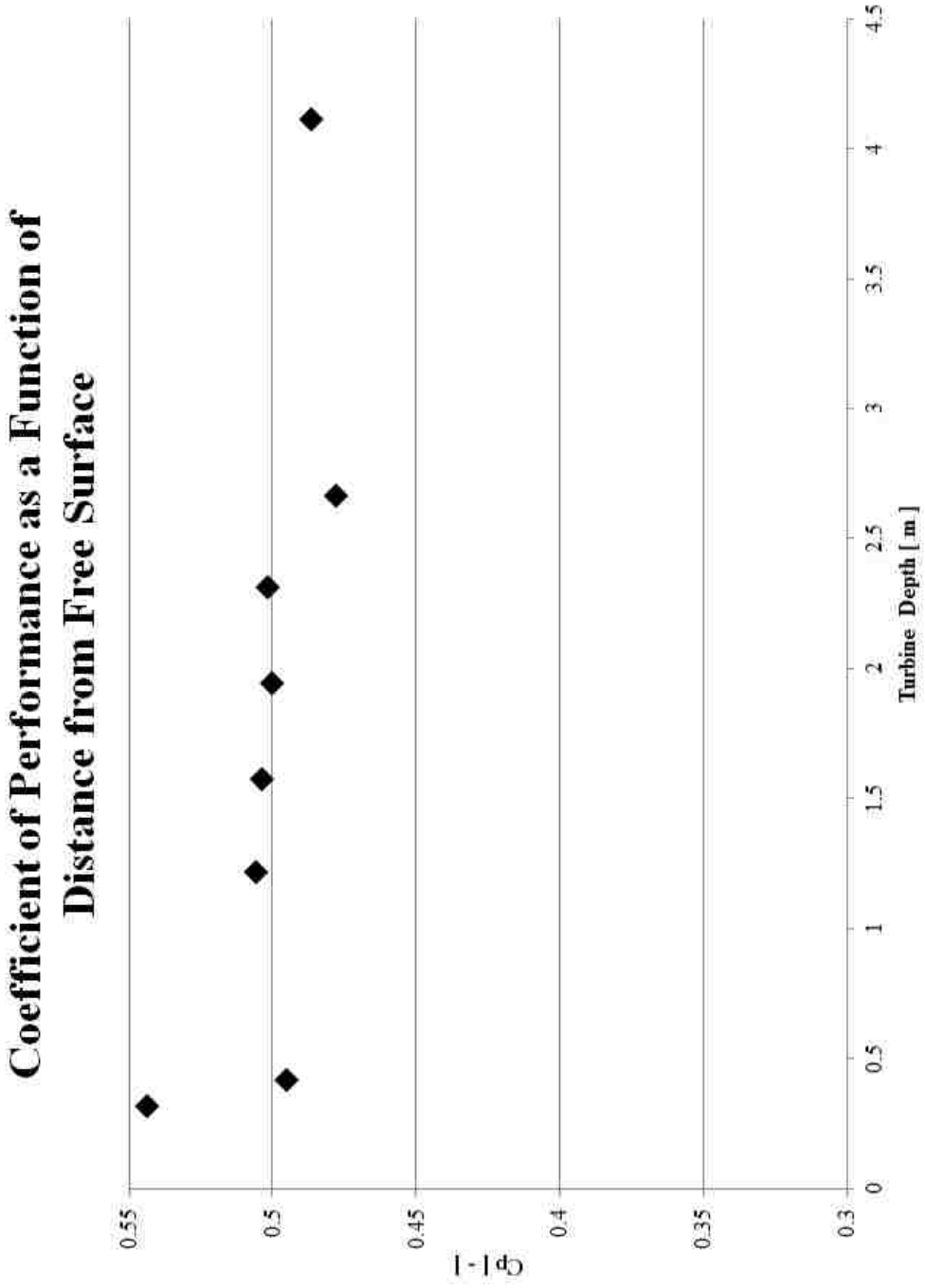

Figure 12: Coefficient of Performance as a Function of Distance below Free Surface

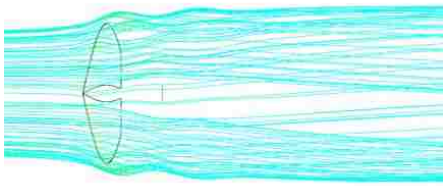

(a)

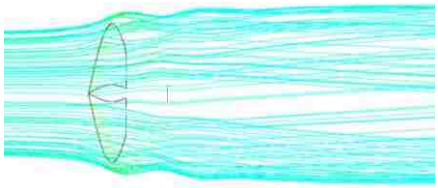

(b)

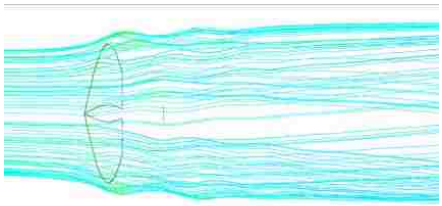

(c)

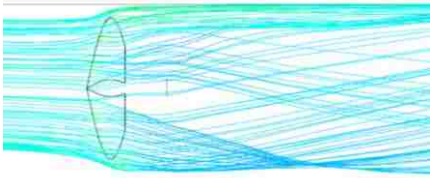

(d)

$h =$ (a) 4.115 m (162 in), (b) 1.943 m (76.5 in), (c) 0.4191 m (16.5 in), (d) 0.3175 m (12.5 in)

Figure 13: Streamlines for Various Values of Turbine Depth

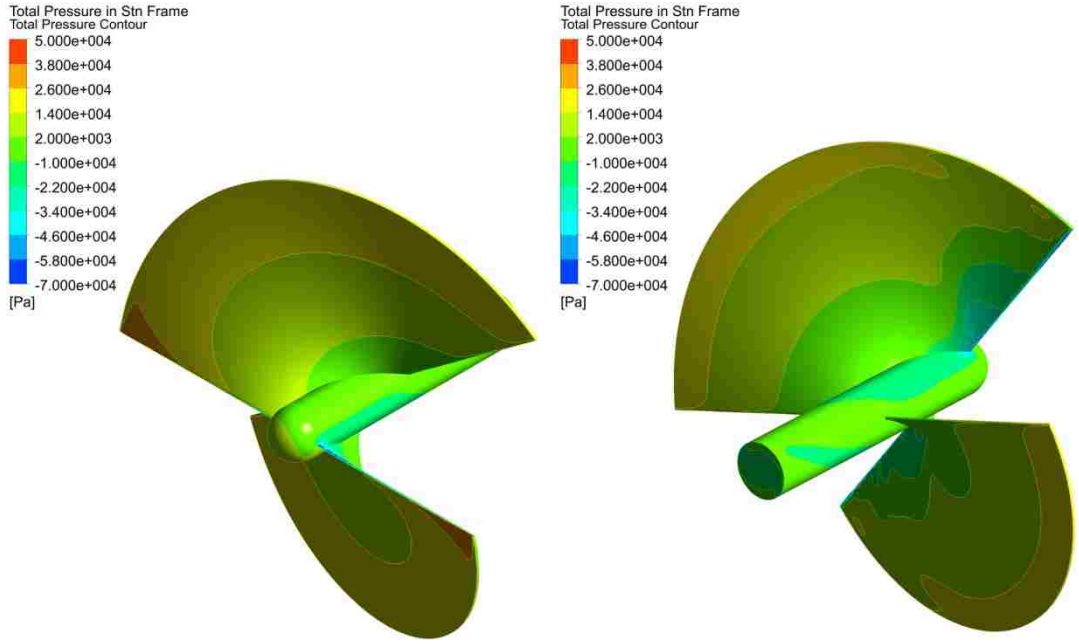
Total Pressure in Stn Frame
Total Pressure Contour
5.000e+004
3.800e+004
2.600e+004
1.400e+004
2.000e+003
-1.000e+004
-2.200e+004
-3.400e+004
-4.600e+004
-5.800e+004
-7.000e+004
[Pa]
Total Pressure in Stn Frame
Total Pressure Contour
5.000e+004
3.800e+004
2.600e+004
1.400e+004
2.000e+003
-1.000e+004
-2.200e+004
-3.400e+004
-4.600e+004
-5.800e+004
-7.000e+004
[Pa]

(a)

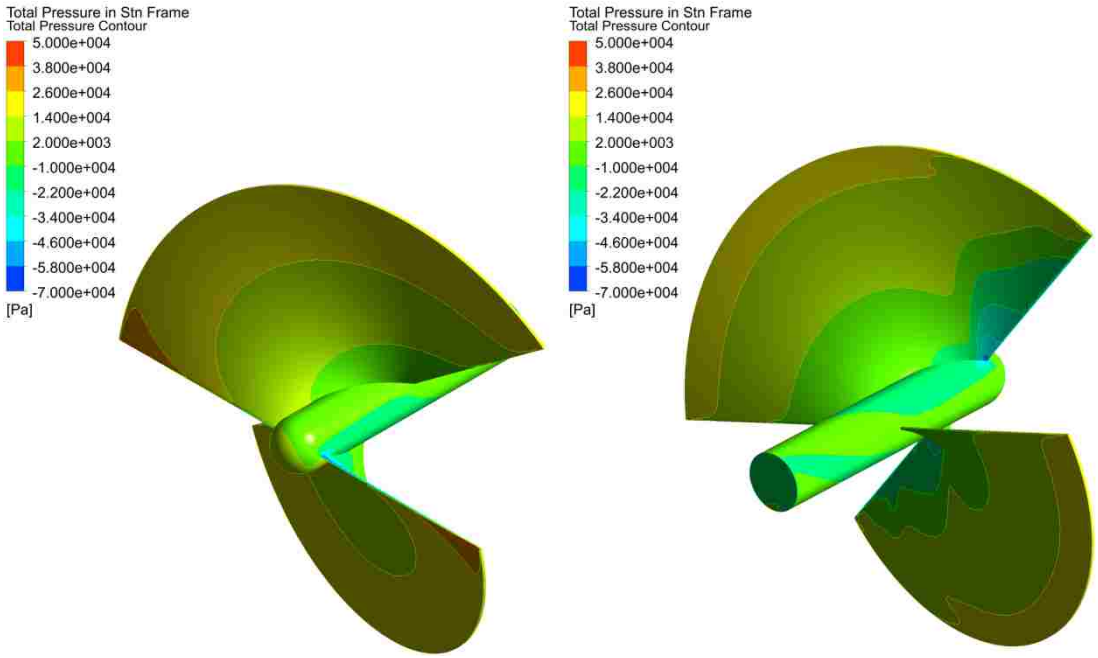
Total Pressure in Stn Frame
Total Pressure Contour
5.000e+004
3.800e+004
2.600e+004
1.400e+004
2.000e+003
-1.000e+004
-2.200e+004
-3.400e+004
-4.600e+004
-5.800e+004
-7.000e+004
[Pa]
Total Pressure in Stn Frame
Total Pressure Contour
5.000e+004
3.800e+004
2.600e+004
1.400e+004
2.000e+003
-1.000e+004
-2.200e+004
-3.400e+004
-4.600e+004
-5.800e+004
-7.000e+004
[Pa]

(b)

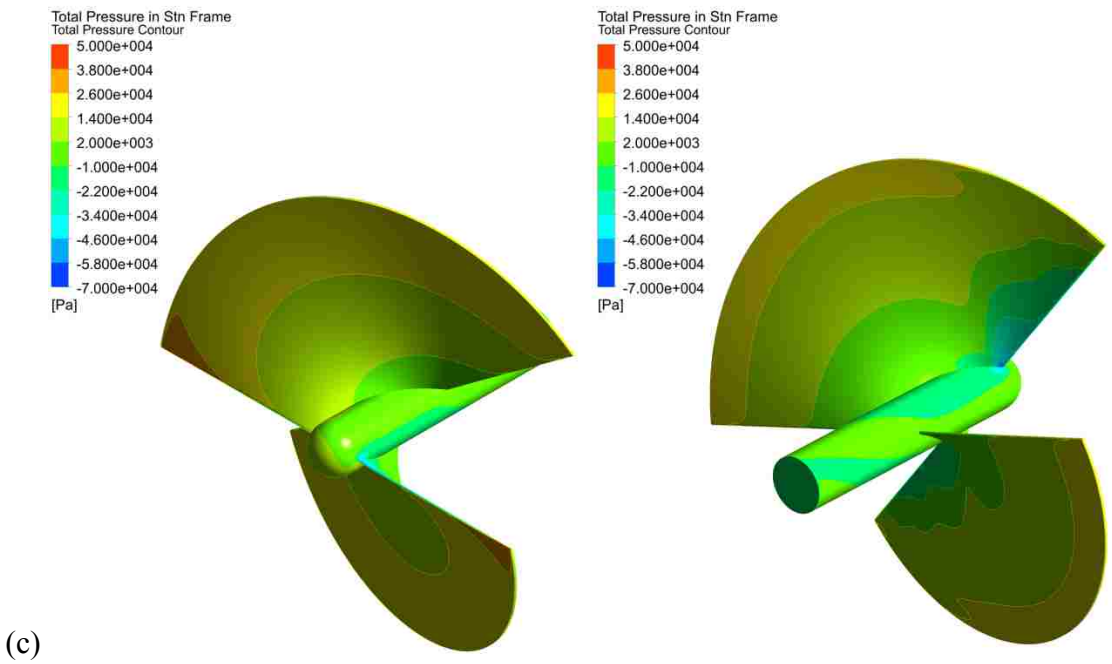

(c)

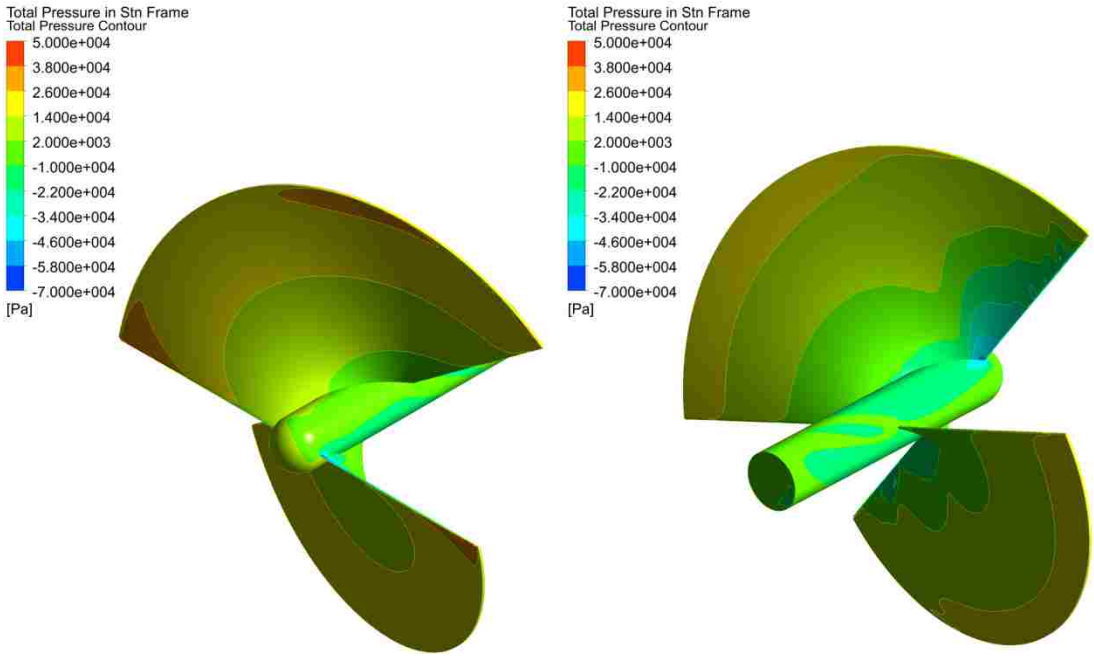

(d)

$h =$ (a) 4.115 m (162 in), (b) 1.219 m (48 in), (c) 0.4191 m (16.5 in), (d) 0.3175 m (12.5 in)

Figure 14: Pressure Contours for Various Values of Turbine Depth

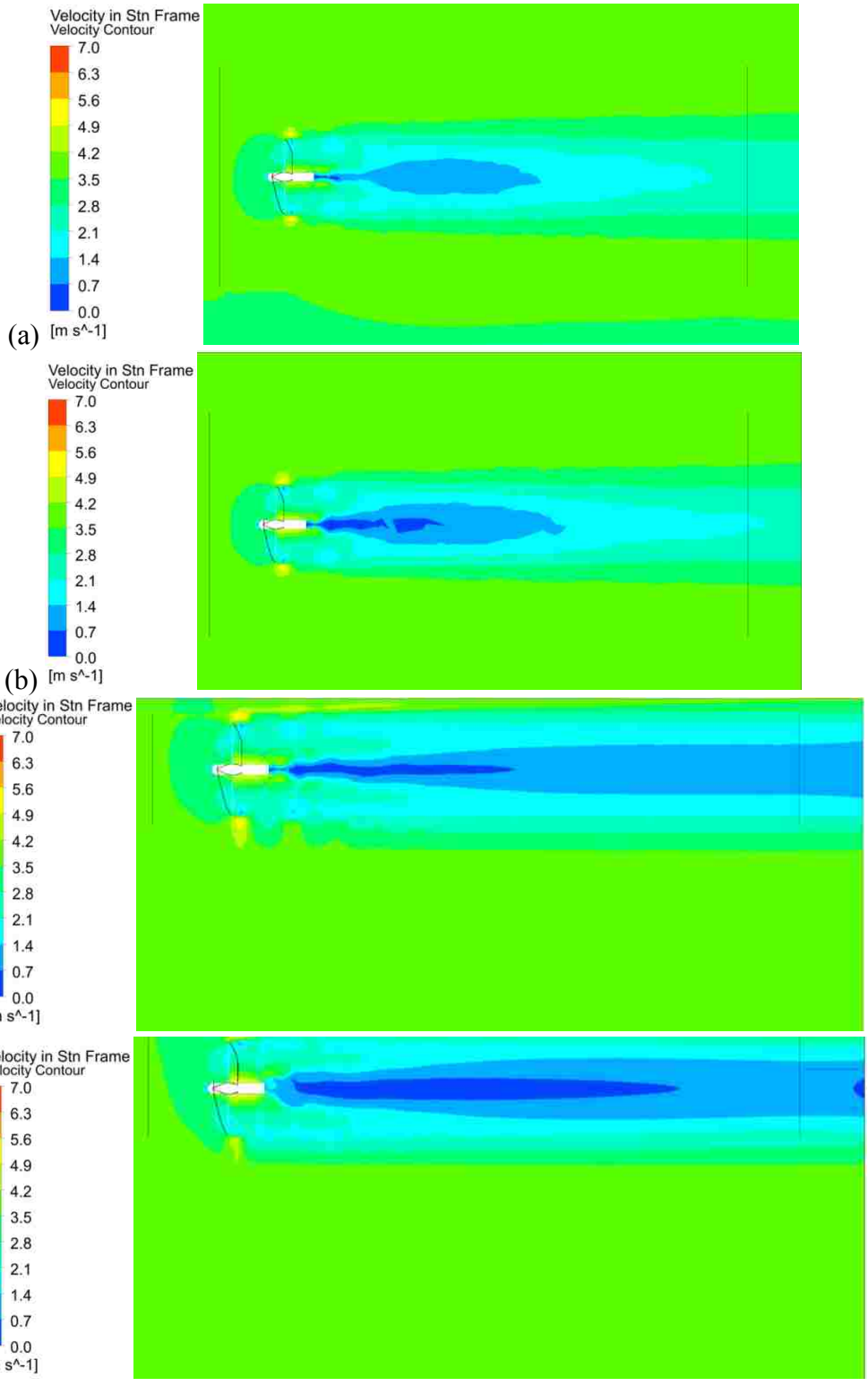

$h =$ (a) 4.115 m (162 in), (b) 1.219 m (48 in), (c) 0.4191 m (16.5 in), (d) 0.3175 m (12.5 in)

Figure 15: Velocity Contours for Various Values of Turbine Depth

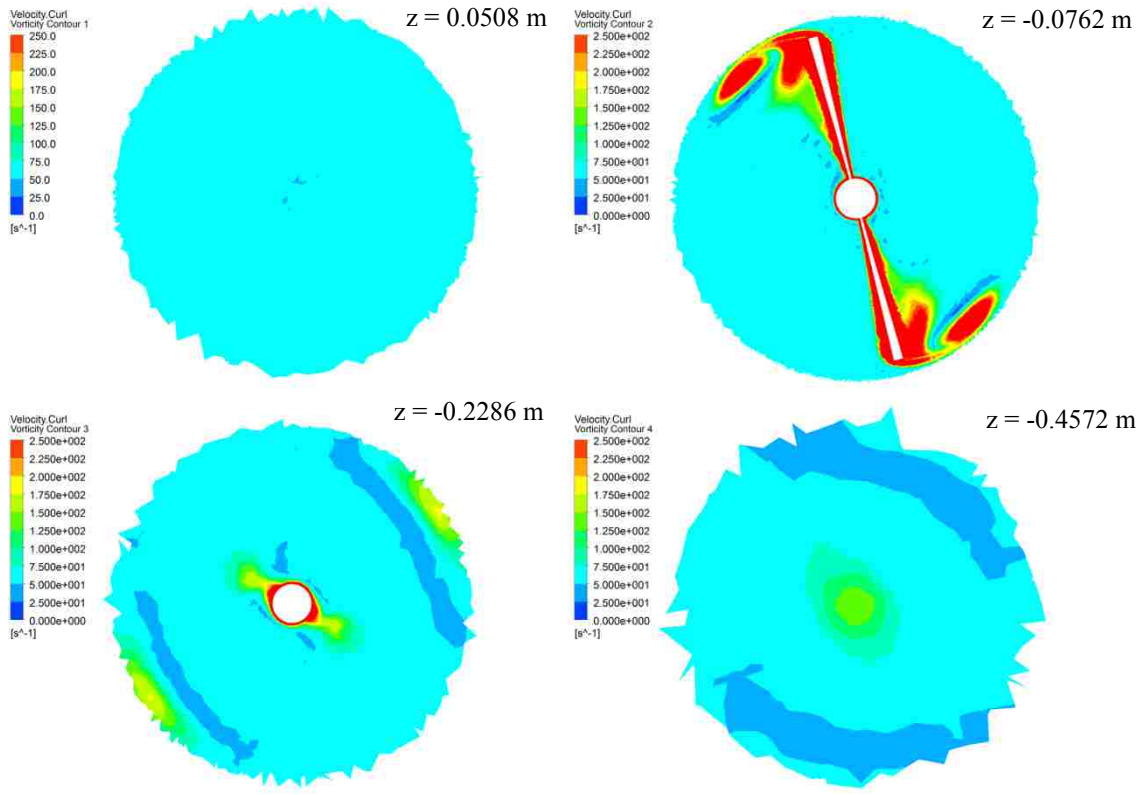
Velocity Curl
Vorticity Contour 1
250.0
225.0
200.0
175.0
150.0
125.0
100.0
75.0
50.0
25.0
0.0
[s^-1]
z = 0.0508 m
Velocity Curl
Vorticity Contour 2
2.500e+002
2.250e+002
2.000e+002
1.750e+002
1.500e+002
1.250e+002
1.000e+002
7.500e+001
5.000e+001
2.500e+001
0.000e+000
[s^-1]
z = -0.0762 m
Velocity Curl
Vorticity Contour 3
2.500e+002
2.250e+002
2.000e+002
1.750e+002
1.500e+002
1.250e+002
1.000e+002
7.500e+001
5.000e+001
2.500e+001
0.000e+000
[s^-1]
z = -0.2286 m
Velocity Curl
Vorticity Contour 4
2.500e+002
2.250e+002
2.000e+002
1.750e+002
1.500e+002
1.250e+002
1.000e+002
7.500e+001
5.000e+001
2.500e+001
0.000e+000
[s^-1]
z = -0.4572 m

(a)

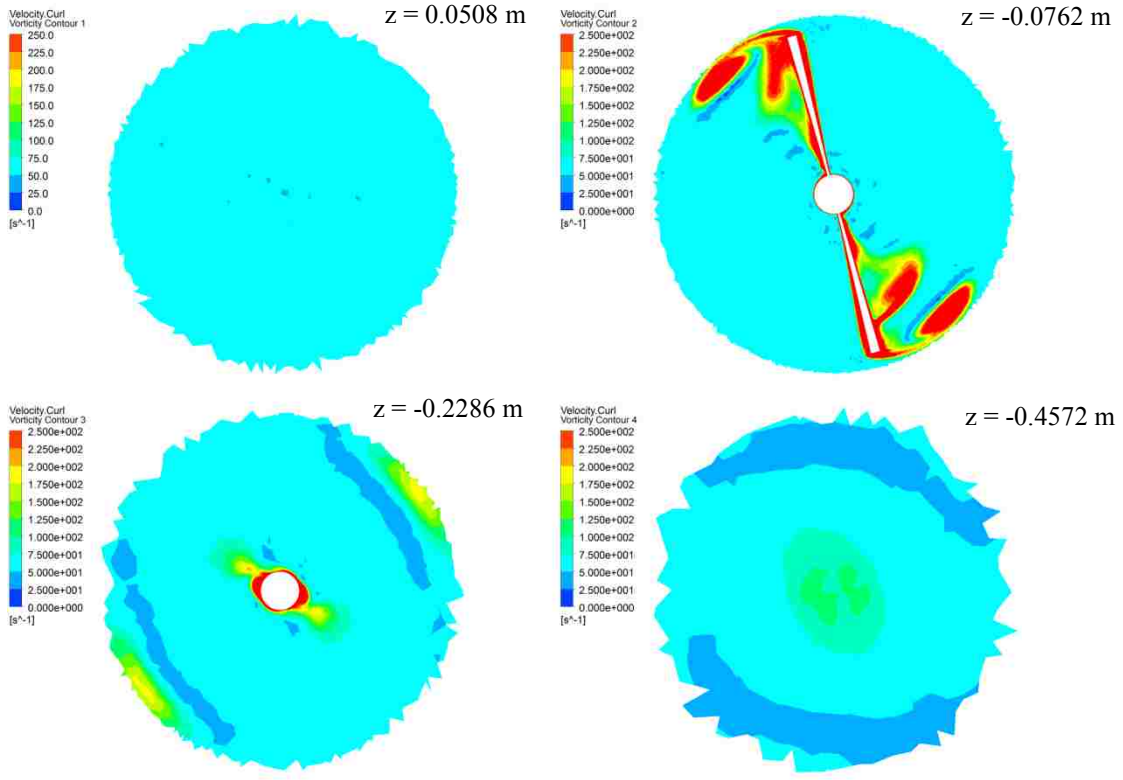
Velocity Curl
Vorticity Contour 1
250.0
225.0
200.0
175.0
150.0
125.0
100.0
75.0
50.0
25.0
0.0
[s^-1]
z = 0.0508 m
Velocity Curl
Vorticity Contour 2
2.500e+002
2.250e+002
2.000e+002
1.750e+002
1.500e+002
1.250e+002
1.000e+002
7.500e+001
5.000e+001
2.500e+001
0.000e+000
[s^-1]
z = -0.0762 m
Velocity Curl
Vorticity Contour 3
2.500e+002
2.250e+002
2.000e+002
1.750e+002
1.500e+002
1.250e+002
1.000e+002
7.500e+001
5.000e+001
2.500e+001
0.000e+000
[s^-1]
z = -0.2286 m
Velocity Curl
Vorticity Contour 4
2.500e+002
2.250e+002
2.000e+002
1.750e+002
1.500e+002
1.250e+002
1.000e+002
7.500e+001
5.000e+001
2.500e+001
0.000e+000
[s^-1]
z = -0.4572 m

(b)

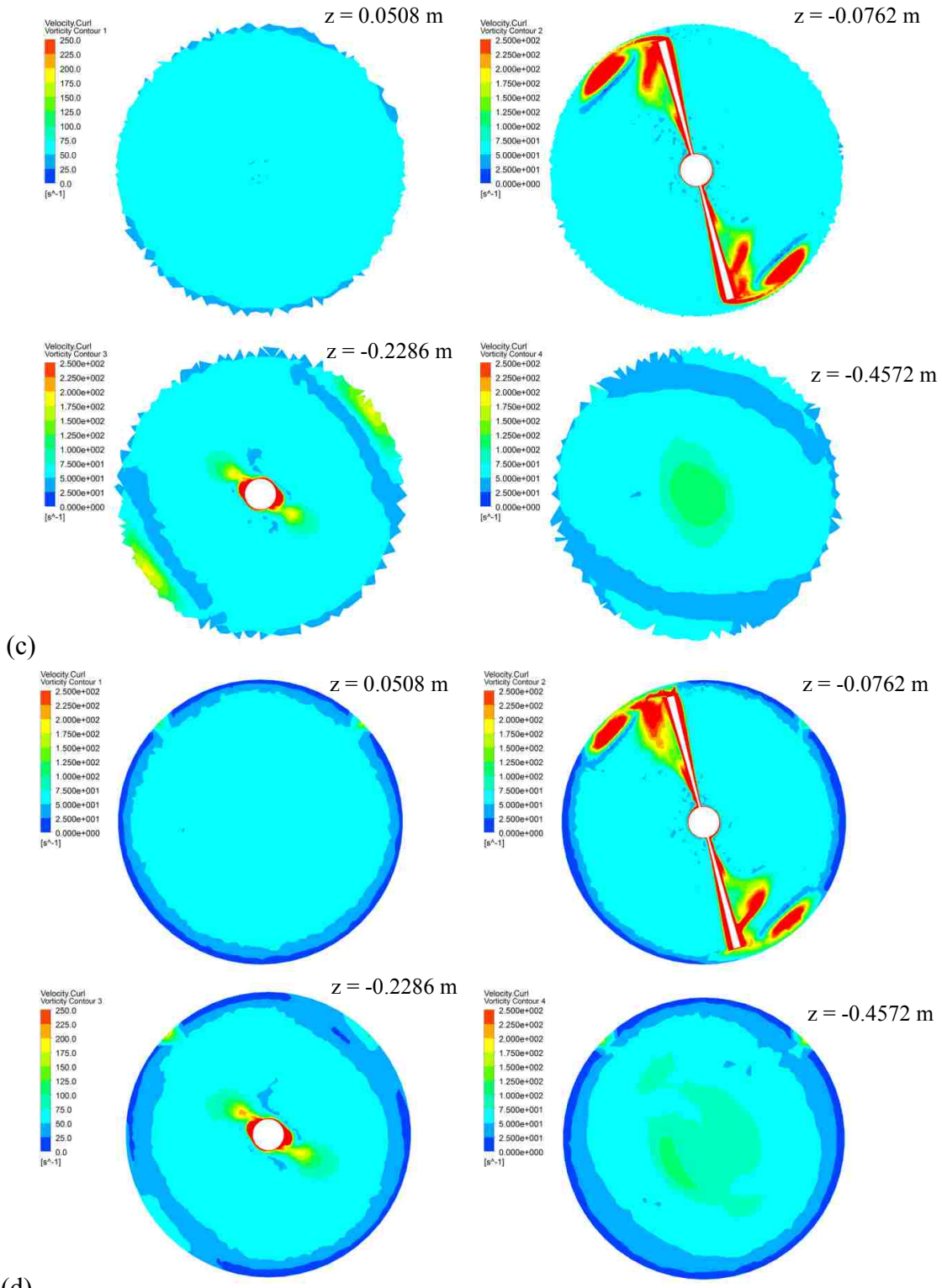

$h =$ (a) 4.115 m (162 in), (b) 1.943 m (76.5 in), (c) 0.4191 m (16.5 in), (d) 0.3175 m (12.5 in)

Figure 16: Vorticity Contours for Various Values of Turbine Depth

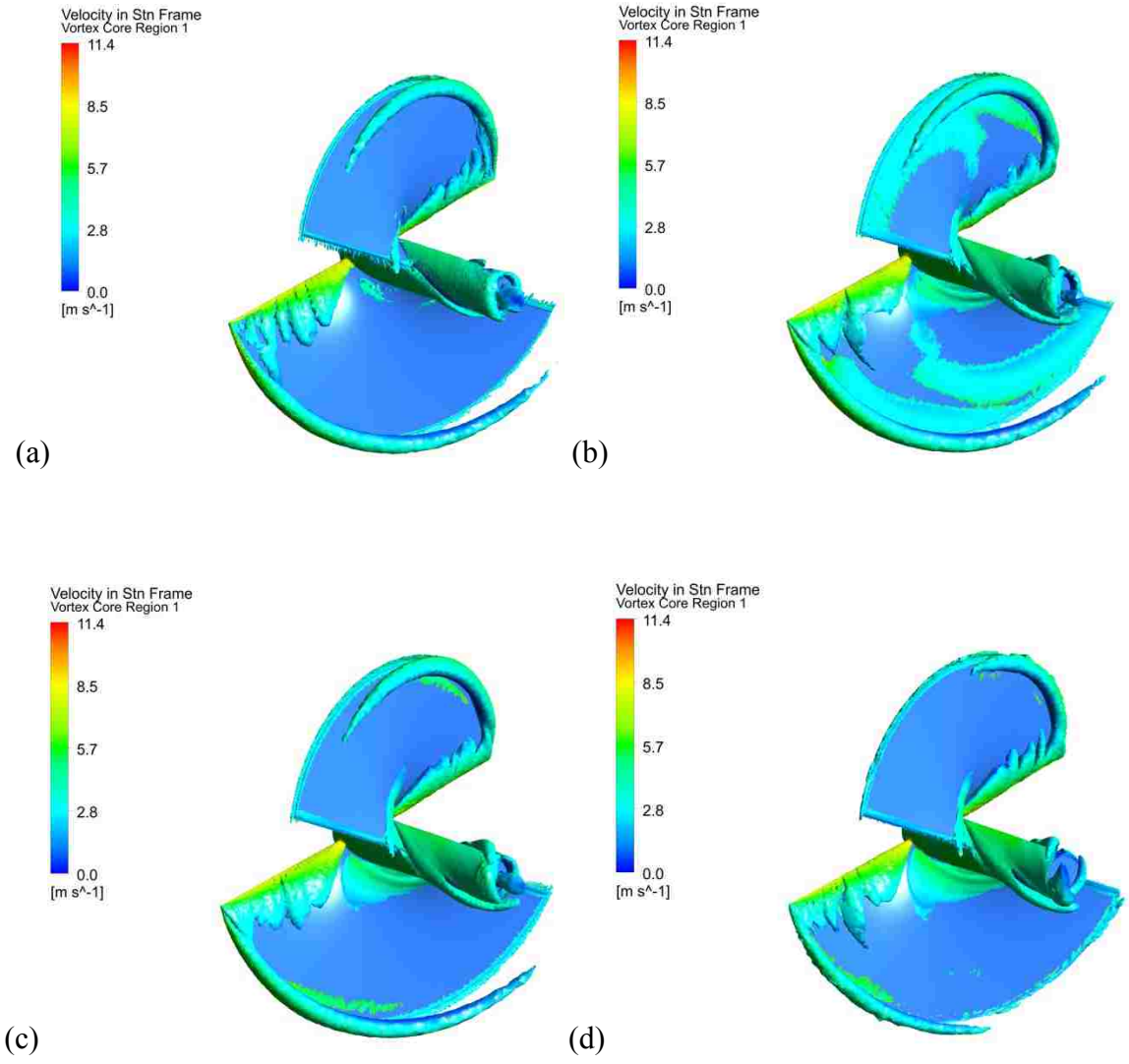

$h =$ (a) 4.115 m (162 in), (b) 1.575 m (62 in), (c) 0.4191 m (16.5 in), (d) 0.3175 m (12.5 in)

Figure 17: Vortex Ropes for Various Values of Turbine Depth

4.3 Outlet Effects and Spectral Convergence

To check the geometrical independence of results, as mentioned in 4.1 Blockage Ratio Results, the distance downstream of the turbine is increased from 3.81 to 4.572 meters (150 to 180 inches) for two values of blockage ratio, and the coefficient of performance values for both geometries are compared. For both values of blockage ratio, the difference in reported coefficient of performance values is less than one percent, indicating that the turbine is sufficiently far from the outlet. The details of this comparison can be seen in Table 1.

Blockage Ratio [-]	C_p [-] for Downstream Distance of 3.81 m (150 in)	C_p [-] for Downstream Distance of 4.572 m (180 in)	Difference [%]
0.50	0.5866	0.5865	0.02
0.05	0.5089	0.5083	0.12

Table 1: Comparison of Results for Geometrical Convergence

The blockage ratio results are also checked for mesh convergence, as it is possible that the accuracy of one set of results could be dependent upon mesh size. Figure 18 displays data for the two mesh sizes mentioned earlier. The results obtained for these two mesh sizes differ only slightly from one another, with the largest difference being only 2.33 percent. Thus, the results obtained for the effects of blockage ratio are independent of mesh size.

The free surface results are not checked for mesh convergence since doing so would require computational power that is not available for this study.

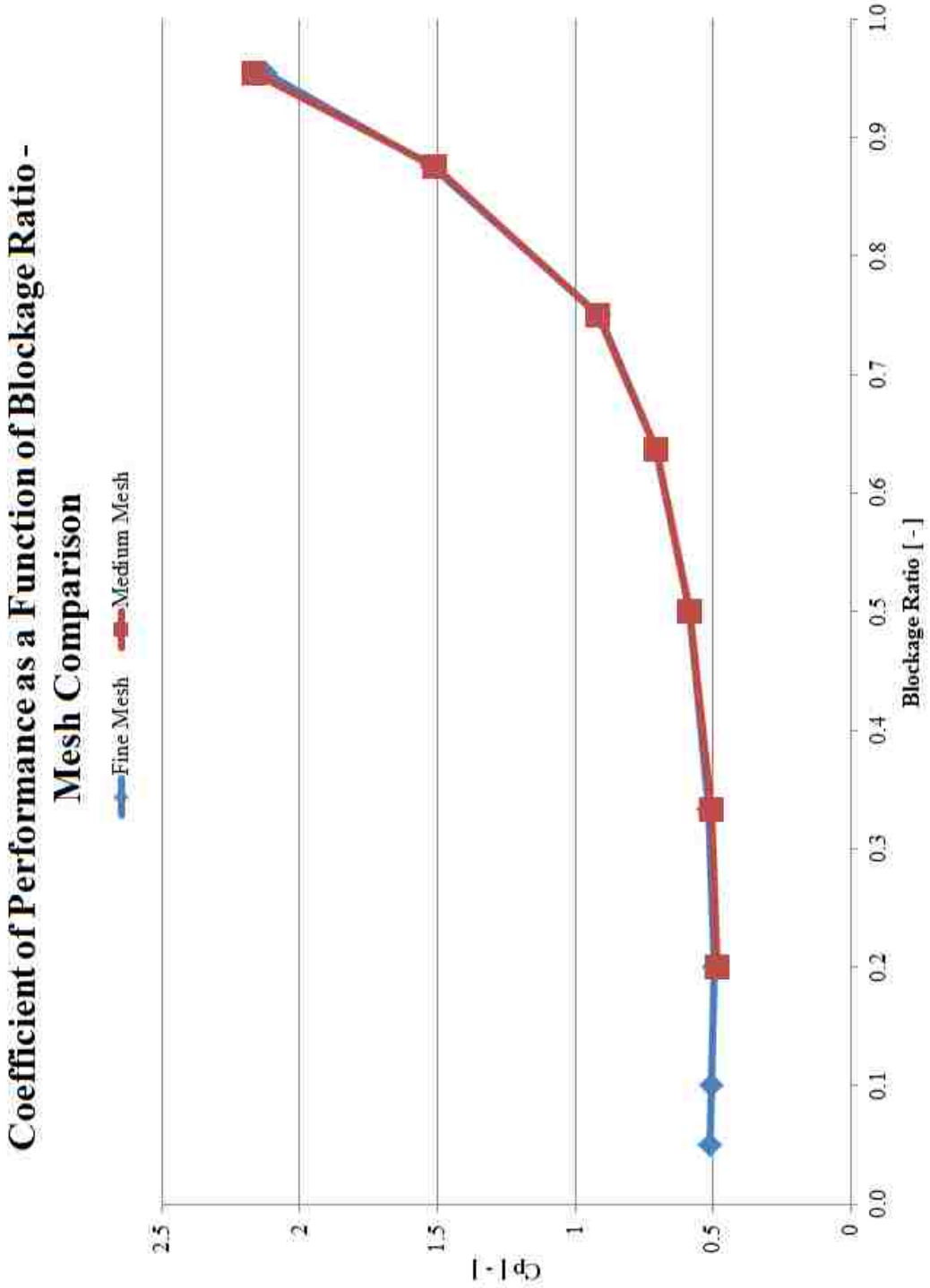

Figure 18: Comparison of Blockage Ratio Results for Mesh Convergence

5. Conclusions

The following conclusions have been drawn for a channel flow velocity of 3.5 m/s, a turbine rotation rate of 250 RPM, and the turbine blade design employed in this study.

The coefficient of performance of a hydrokinetic turbine varies insignificantly for blockage ratios less than approximately 0.4. For values of blockage ratio larger than 0.4, the coefficient of performance increases considerably, especially for values of blockage ratio approaching 1. At such values, the coefficient of performance graphically appears to tend towards a vertical asymptote, though such results are not physically plausible.

The distance of a turbine from the free surface of a channel does not appear to affect its coefficient of performance, except when the turbine is placed very close to the free surface; at such distances, the coefficient of performance increases. However, the computational domain or mesh employed in this study may not be sufficient for obtaining accurate results. It is suggested that further study be performed on this topic using either a finer mesh or a two-phase domain that includes air above the free surface of the river.

Anyone wishing to determine the effects of other parameters on turbine performance should use a maximum blockage ratio of 0.4 so as to avoid the effects of this parameter. Anyone wishing to install a hydrokinetic turbine should seek a venue where the blockage ratio is as large as reasonably possible.

6. Bibliography

[1] K. H. Fasol, "A Short History of Hydropower Control," *IEEE Control Systems Magazine,* pp. 68-76, August 2002.

[2] U.S. Department of the Interior, "The History of Hydropower Development in the United States," Bureau of Reclamation, 12 August 2009. [Online]. Available: http://www.usbr.gov/power/edu/history.html. [Accessed 19 June 2013].

[3] J. J. Conti, Annual Energy Outlook 2010: With Projections to 2035, U.S. Energy Information Administration, Office of Integrated Analysis and Forecasting, U.S. Department of Energy, 2010.

[4] K. E. McCarthy, "Pros and Cons of Hydropower," Connecticut Office of Legislative Research, 4 October 2010. [Online]. Available: http://cga.ct.gov/2010/rpt/2010-R-0401.htm. [Accessed 19 June 2013].

[5] M. J. Khan, G. Bhuyan, M. T. Iqbal and J. E. Quaicoe, "Hydrokinetic energy conversion systems and assessment of horizontal and vertical axis turbines for river and tidal applications: A technology status review," *Applied Energy,* vol. 86, no. 10, pp. 1823-1835, 2009.

[6] L. Myers and A. S. Bahaj, "Power output performance characteristics of a horizontal axis marine current turbine," *Renewable Energy,* vol. 31, no. 2, pp. 197-208, 2006.

[7] W. M. J. Batten, A. S. Bahaj, A. Molland and J. R. Chaplin, "Hydrodynamics of marine current turbines," *Renewable Energy,* vol. 31, no. 2, pp. 249-256, 2006.

[8] I. S. Hwang, Y. H. Lee and S. J. Kim, "Optimization of cycloidal water turbine and the performance improvement by individual blade control," *Applied Energy,* vol. 86, no. 9, pp. 1532-1540, 2009.

[9] C. A. Consul, R. H. G. Wilden, E. Ferrer and M. D. McCulloch, in *Proceedings of the 8th European Wave and Tidal Energy Conference*, Uppsala, Sweden, 2009.

[10] S. L. Dixon, Fluid Mechanics and Thermodynamics of Turbomachinery, 5th Ed., Burlington, MA: Elsevier Butterworth-Heinemann, 2005.

[11] C. Garrett and P. Cummins, "The efficiency of a turbine in a tidal channel," *Journal of Fluid Mechanics,* vol. 588, pp. 243-251, 2007.

[12] O. Zikanov, Essential Computational Fluid Dynamics, Hoboken, NJ: Wiley, 2010.

[13] W. C. Schleicher, J. D. Riglin, Z. A. Kraybill, A. Oztekin and R. C. Klein, Jr., "Design and Simulation of a Micro Hydrokinetic Turbine," in *Proceedings of the 1st Marine Energy Technology Symposium*, Washington, D.C., 2013.

[14] F. R. Menter, "Two-Equation Eddy-Viscosity Turbulence Models for Engineering Applications," *AIAA Journal,* vol. 32, no. 8, pp. 1598-1605, 1994.

[15] ANSYS, Inc., "Theory Guide," 2009.

7. Vita

Peter Creciun was born in Norristown, PA, on August 31, 1990, to Michael and Mary Lee Creciun. He graduated from Kennedy-Kenrick Catholic High School in Norristown in 2008, and he received his Bachelor of Science Degree in Mechanical Engineering at Lehigh University in Bethlehem, PA, in 2012. In 2013 he received his Master of Science Degree in Mechanical Engineering from Lehigh University.